

ANALYSIS OF MAGNETIC FIELD EFFECT ON PULSATING BLOOD FLOW IN ARTERIES

SADIA NOON OISHE

M.Sc. Engineering THESIS



**DEPARTMENT OF MECHANICAL ENGINEERING
MILITARY INSTITUTE OF SCIENCE AND TECHNOLOGY
DHAKA, BANGLADESH**

APRIL 2022

ANALYSIS OF MAGNETIC FIELD EFFECT ON PULSATING BLOOD
FLOW IN ARTERIES

SADIA NOON OISHE (SN. 0418180007)

A Thesis Submitted in Partial Fulfillment of the Requirements for the Degree of Masters of
Science in Mechanical Engineering



DEPARTMENT OF MECHANICAL ENGINEERING
MILITARY INSTITUTE OF SCIENCE AND TECHNOLOGY
DHAKA, BANGLADESH

APRIL 2022

ANALYSIS OF MAGNETIC FIELD EFFECT ON PULSATING BLOOD
FLOW IN ARTERIES

M.Sc. Engineering Thesis

By

SADIA NOON OISHE (SN.0418180007)

Approved as to style and content by the Board of Examination on 20 April 2022:

.....
Dr. Dipak Kanti Das
Professor of Mechanical Engineering
MIST, Dhaka
Chairman (Supervisor)
Board of Examination

.....
Dr. A.B.M. Toufique Hasan
Professor of Mechanical Engineering
BUET, Dhaka
Member (External)
Board of Examination

.....
Dr. R. G. M. Hasan
Professor of Mechanical Engineering
MIST, Dhaka
Member
Examination

.....
Brigadier General Md. Omar Faruque, afwc, psc
MIST, Dhaka
Head of the Department
Member, (Ex-officio)

Department of Mechanical Engineering MIST, Dhaka

ANALYSIS OF MAGNETIC FIELD EFFECT ON PULSATING BLOOD
FLOW IN ARTERIES

DECLARATION

I hereby declare that the study reported in this thesis is my original work and has not been submitted before anywhere for any degree or other purposes. Further, I certify that the intellectual content of this thesis is the product of my own work and that all the assistance received in preparing this thesis and sources have been acknowledged and/or cited in the reference section.

.....

Sadia Noon Oishe

Department of Mechanical Engineering MIST, Dhaka

NUMERICAL ANALYSIS OF MAGNETIC FIELD EFFECT ON
PULSATING BLOOD FLOW IN ARTERIES

A Thesis

By

Sadia Noon Oishe

DEDICATION

Dedicated to my mother Sharia Laila for supporting me.

ACKNOWLEDGEMENTS

All praise be to Allah, the Cherisher and Sustainer of the worlds for His kindness and blessings for allowing me to do this colossal work and finally materialize it.

The author expresses her deepest gratitude and profound indebtedness to her supervisor, Professor Dr. Dipak Kanti Das, Department of Mechanical Engineering, MIST, Dhaka, for his continuous supervision, valuable opinions, and motivation for research work all through the time. His regular support and direction made this research work possible and fruitful at every stage.

The author is also thankful to Brig Gen Md Humayun Kabir Bhuiyan, psc, Dean, Department of Mechanical Engineering, MIST for his encouragement throughout the whole course. Special gratitude to Brig Gen Md. Omar Faruque, afwc, psc, Head, Department of Mechanical Engineering, MIST for his guidance at every step is duly acknowledged. The author would also like to thank Professor Dr. R. G. M Hasan for supporting me academically and personally and Professor Dr. A.B.M. Toufique Hasan for his valuable guidance and thanks to all Department of Mechanical Engineering, MIST for their cooperation in the successful fulfillment of the work.

Finally, the author would like to express sincere thanks to all the beautiful people who stayed beside them when truly needed their support for the successful completion of this work.

ABSTRACT

ANALYSIS OF MAGNETIC FIELD EFFECT ON PULSATING BLOOD FLOW IN ARTERIES

Cardiovascular diseases including strokes, heart attacks, Stenosis, and atherosclerosis are considered the leading cause of death over the globe. The aorta, coronary, carotid, and femoral arteries are the most commonly impacted arteries. It's a crucial field of study for blood flow behavior. For many years, researchers have experimented with various numerical strategies to entice clinicians to trust their colorful contours. In recent, the impact of magnetic fields on blood flow is one of the developing approaches to treating different types of diseases. However, the efficiency of MHD capture is still unclear, and there is less systematic strategy to understand the flow behavior of blood. In this study, a simulation-based three-dimensional human aorta (brachiocephalic trunk, left subclavian, and left carotid) with transient conditions is analyzed to predict changes in blood flow distribution and flow patterns under with and without magnetic field conditions. Blood is modeled as non-Newtonian fluids along with plasma. VOF modeling for multiphase flow is used to mix RBC and plasma to predict the pulsating condition for the flow. Moreover, 1 Tesla magnetic field is applied to the selected section of the aorta. For simulation purposes, ANSYS Fluent software is used to identify the values for velocity, pressure, and wall shear force to understand the flow behavior of blood. The result shows that velocity, pressure, and wall shear stress are affected by exposure to MHD. By applying MHD, due to the freezing effect, the flow velocity slows down by about .035% while pressure increases by 9%, wall shear stress increases by 1.46% as well as mass flow.

Keywords: *Human aorta, Non-Newtonian Blood flow, VOF, MHD.*

সারসংক্ষেপ

ANALYSIS OF MAGNETIC FIELD EFFECT ON PULSATING BLOOD FLOW IN ARTERIES

স্ট্রোক, হার্ট অ্যাটাক, স্টেনোসিস এবং এথেরোস্কেলেরোসিস সহ কার্ডিওভাসকুলার রোগগুলিকে বিশ্বজুড়ে মৃত্যুর প্রধান কারণ হিসাবে বিবেচনা করা হয়। অ্যাওর্টা, করোনারি, ক্যারোটিড এবং ফেমোরাল ধমনী হল সবচেয়ে বেশি প্রভাবিত ধমনী। এটি রক্ত প্রবাহ আচরণের জন্য অধ্যয়নের একটি গুরুত্বপূর্ণ ক্ষেত্র। বহু বছর ধরে গবেষকরা চিকিৎসকদের তাদের রঙিন রূপের উপর আস্থা রাখতে প্রলুব্ধ করার জন্য বিভিন্ন সংখ্যাসূচক কৌশল নিয়ে পরীক্ষা করেছেন। সাম্প্রতিক সময়ে রক্ত প্রবাহের উপর চৌম্বকীয় ক্ষেত্রের প্রভাব বিভিন্ন ধরণের রোগের চিকিৎসার জন্য উন্নয়নশীল পদ্ধতির একটি। MHD কার্যকারিতা এখনও অস্পষ্ট এবং রক্তের প্রবাহের আচরণ বোঝার জন্য কম পদ্ধতিগত কৌশল রয়েছে। এই গবেষণায় ক্ষণস্থায়ী অবস্থার সাথে একটি সিমুলেশন-ভিত্তিক ত্রি-মাত্রিক মানব মহাধমনী (ব্র্যাকিওসেফালিক ট্রাঙ্ক, বাম সাবক্ল্যাভিয়ান এবং বাম ক্যারোটিড) বিশ্লেষণ করা হয় যাতে চৌম্বকীয় ক্ষেত্রের অবস্থার সাথে এবং ছাড়াই রক্ত প্রবাহ বন্টন এবং প্রবাহের ধরণগুলির পরিবর্তনের পূর্বাভাস দেওয়া হয়। রক্তকে প্লাজমার সাথে অ-নিউটনিয়ান তরল হিসাবে মডেল করা হয়। মাল্টিফেজ প্রবাহের জন্য VOF মডেলিং প্রবাহের জন্য স্পন্দনশীল অবস্থার পূর্বাভাস দিতে RBC এবং প্লাজমা মিশ্রিত করতে ব্যবহৃত হয়। তাছাড়া, ১ টেসলা চৌম্বক ক্ষেত্র মহাধমনীর নির্বাচিত অংশে প্রয়োগ করা হয়। সিমুলেশন উদ্দেশ্যে, ANSYS ফ্লুয়েন্ট সফটওয়্যার রক্তের প্রবাহের আচরণ বোঝার জন্য বেগ, চাপ এবং প্রাচীর শিয়ার বলের মান সনাক্ত করতে ব্যবহৃত হয়। ফলাফল দেখায় যে বেগ, চাপ এবং প্রাচীর শিয়ার স্ট্রেস MHD-এর এক্সপোজার দ্বারা প্রভাবিত হয়। MHD প্রয়োগ করে, হিমায়িত প্রভাবের কারণে, প্রবাহের বেগ প্রায় ০.০৩৫% হ্রাস পায় যখন চাপ ৯% বৃদ্ধি পায়, ওয়াল শিয়ার স্ট্রেস ১.৪৬% বৃদ্ধি পায় সেইসাথে ভর প্রবাহও বৃদ্ধি পায়।

LIST OF MAIN NOTATIONS

U	Velocity component in x-direction, m/s
V	Velocity component in y-direction, m/s
W	Velocity component in z-direction, m/s
G	Gravity, m^2/s
H	Height, m
a_x	Acceleration in x-direction, m^2/s
P_0	Pressure in the center, Pa
P	Pressure, Pa
ρ	Density, kg/m^3
\mathcal{T}_{xx}	Shear stress in x-direction, Pa
\mathcal{T}_{yy}	Shear stress in y-direction, Pa
\mathcal{T}_{zz}	Shear stress in z-direction, Pa
Q	Total velocity, m/s
ω_x	Rotation in x-axis, s^{-1}
ω_y	Rotation in y-axis, s^{-1}
ω_z	Rotation in z-axis, s^{-1}
\mathcal{V}	Kinematic viscosity, m^2/s
\vec{E}	Electric field,
ρ_c	Charge density, c/m^3
ϵ_0	Electric permittivity of free space
\vec{B}	Magnetic field

∇	Curl operator
μ_0	Magnetic permeability of free space, henries/m
\vec{j}	Current density
C	Speed of light, m/s
Q	Column force
\vec{F}	Lorentz' force
V_0	Volume
\vec{f}	Lorentz's force per unit volume
T	Local time within each period

Abbreviations

FEM	Finite Element Method
MHD	Magneto-Hydro-Dynamics
BFD	Biomagnetic Fluid Dynamics
BT	Brachiocephalic Trunk
LS	Left Subclavian
LC	Left Carotid
3D	Three Dimensional
NNF	Non-Newtonian Factor
TAWSS	Time average wall shear stress
CFD	Computational Fluid Dynamics
UDF	User Define File
VOF	Volume of Fraction
Cps	Centipoise

LIST OF FIGURES

Figure. 1.1:	Particles of blood	2
Figure. 1.2:	Blood sediment	3
Figure. 1.3:	Hemoglobin tetramer	5
Figure. 1.4:	Structure of hemoglobin	5
Figure. 1.5:	Human heart	7
Figure. 3.1:	Control volume	15
Figure. 3.2:	Stress vs strain curve of Newtonian and non-Newtonian materials	19
Figure. 4.1:	A three-dimensional design with inlet and outlet diameter	26
Figure. 4.2:	Design of selected human arteries with dimension (two-dimensional)	27
Figure. 4.3:	Design of selected human arteries in isometric view	28
Figure. 4.4:	A cross-sectional plane in xy-direction	28
Figure. 4.5:	Three-dimensional meshing domain	29
Figure. 4.6:	Inlet velocity profile	30
Figure. 4.7:	(a) Meshing view (b) Close view of meshing around the arc	33
Figure. 4.8:	Mesh sensitivity test result	34
Figure. 5.1:	(a) Geometry taken from Morries et al (2005) (b) Descending aorta data from Morries et al. (2005)	36
Figure. 5.2:	Comparison of the present study in terms of velocity at the outlet with Morries et al. (2005)	36
Figure. 5.3:	Outlet pressure profile with time (a) Single phase (without VOF model) (b) Two phase (VOF model)	37
Figure. 5.4:	(a) Graph from Altintas and Ozkol (2015) (b) velocity vs position	38
Figure. 5.5:	Selected planes with inlet and outlets	39
Figure. 5.6:	Inlet velocity contour	40
Figure. 5.7:	Outlet velocity contour	41
Figure. 5.8:	BT Outlet velocity contour	41
Figure. 5.9:	LC Outlet velocity contour	42
Figure. 5.10:	LS Outlet velocity contour	42

Figure. 5.11:	Plane 1 velocity contour	43
Figure. 5.12:	Plane 2 velocity contour	44
Figure. 5.13:	xy cross-sectional velocity contour	44
Figure. 5.14:	Comparison of velocity profile in line at descending aorta	46
Figure. 5.15:	Outlet velocity profile with time	46
Figure. 5.16:	Comparison of outlet velocity profile with time	47
Figure. 5.17:	Comparison of velocity at $y = 30$ mm (line 1)	47
Figure. 5.18:	Comparison of velocity at $y = -60$ mm (line 3)	48
Figure. 5.19:	Comparison of velocity at line 2	48
Figure. 5.20:	Wall static pressure contour	49
Figure. 5.21:	Inlet pressure contour	49
Figure. 5.22:	Outlet pressure contour	50
Figure. 5.23:	BT Outlet pressure contour	50
Figure. 5.24:	LS Outlet pressure contour	51
Figure. 5.25:	LC Outlet pressure contour	51
Figure. 5.26:	Plane 1 pressure contour	52
Figure. 5.27:	Plane 2 pressure contour	53
Figure. 5.28:	xy cross-sectional plane pressure contour	53
Figure. 5.29:	Pressure distribution for diastolic cycle	54
Figure. 5.30:	Comparing pressure distribution with and without MHD	54
Figure. 5.31:	Wall shear stress without MHD	55
Figure. 5.32:	Wall shear stress with MHD	56
Figure. 5.33:	Velocity streamline	56
Figure. 5.34:	Outlet mass flow	57
Figure. 5.35:	BT Outlet mass flow	57
Figure. 5.36:	LS Outlet mass flow	58
Figure. 5.37:	LC Outlet mass flow	58
Figure. 5.38:	Plane 1 mass flow	59
Figure. 5.39:	Plane 2 mass flow	60
Figure. 5.40:	xy cross-sectional plane mass flow	60

LIST OF TABLES

Table. 3.1	Examples of Newtonian and non-Newtonian fluid	18
Table. 4.1	Properties of blood in Carreau model	25
Table. 4.2	Diameter of aorta section	26
Table. 4.3	Boundary conditions.	29
Table. 4.4	Properties of materials	31
Table. 4.5	Overall system and solver requirement	32
Table. 4.6	Maximum velocity in three types of mesh	34
Table. 5.1	Numerical comparison of velocity due to MHD (1 Tesla)	45

TABLE OF CONTENTS

ACKNOWLEDGEMENTS	i
ABSTRACT	ii
LIST OF MAIN NOTATIONS	
ivi	
LIST OF FIGURES	vi
LIST OF TABLES	viii
CHAPTER 1: INTRODUCTION	1
1.1 General	1
1.1.1 Blood	2
1.1.2 Plasma	3
1.1.3 Blood Cells	4
1.1.4 Red Blood Cells	4
1.1.5 Heart	6
1.2 Objectives of the Thesis	7
1.3 Scope of the Thesis	8
1.4 Structure of the Thesis	9
CHAPTER 2: LITERATURE REVIEW	10
2.1 General	10
2.2 Early Studies of Blood flow	11
2.3 Review of Biomagnetic Fluid Dynamics	12
2.4 This Work	14
CHAPTER 3: RELATED THEORIES	15
3.1 Continuity Equation	15
3.2 Navier-stokes Equation	16
3.3 Viscosity	17
3.4 Newtonian and non-Newtonian Fluid	17

3.5 Wall shear stress	20
3.6 Magneto-Hydro-Dynamics (MHD)	20
3.6.1 Maxwell Equation	20
3.6.1.1 Gauss Law of Electrostatics	20
3.6.1.2 Gauss Law of Magnetism	21
3.6.1.3 Faraday Law	21
3.6.1.4 Ampere Maxwell Law	21
3.6.2 Lorentz' Force	21
3.6.2.1 Volumetric Lorentz' Force	22
CHAPTER 4: GOVERNING EQUATIONS AND COMPUTATIONAL ANALYSIS	24
4.1 Introduction	24
4.2 Governing Equations	24
4.3 Viscosity Model	24
4.4 Selection of Multiphase Modeling	25
4.5 Computational Set-up	25
4.5.1 Human aorta section design	25
4.5.2 Computational geometry and boundary conditions	27
4.5.2.1 Boundary condition for inlet	310
4.5.2.2 User defined function for inlet	31
4.5.3 Parameters for Materials	31
4.5.4 Numerical Scheme	312
4.5.5 Mesh generation	312
4.6 Mesh Sensitivity Test	33
CHAPTER 5: RESULTS AND DISCUSSION	35
5.1 General	35

5.2 Validation of the simulation	35
5.2.1 Validation of velocity	35
5.2.2 Validation of wall shear stress	37
5.2.3 Validation of VOF model	37
5.2.4 Validation of MHD	38
5.3 Computational Results	38
5.3.1 Comparison of velocity	39
5.3.1.1 Velocity at inlet	39
5.3.1.2 Comparison of velocity at outlets	40
5.3.1.3 Comparison of velocity with time	46
5.3.1.4 Comparison of velocity in three different lines	46
5.3.2 Comparison of pressure	49
5.3.2.1 Comparison of pressure with time	54
5.3.3 Comparison of wall shear stress	55
5.3.4 Variation of velocity streamline	56
5.3.5 Comparison of mass flow rate	57
CHAPTER 6: CONCLUSIONS AND RECOMMENDATIONS	61
6.1 Concluding Remarks	61
6.2 Recommendations for Future Work	62
REFERENCES	63

CHAPTER 1

INTRODUCTION

1.1 General

Over the past centuries, fluid dynamics had been studied and developed on a large scale. From inside the human body to the galaxy, fluid dynamics are present. Blood is a specialized fluid that consists of liquid parts and solids particles. The liquid part, called plasma, is made of protein, salts, and water-like substances. More than half of our blood is made of plasma. The solid parts of blood contain white blood cells (WBC), red blood cells (RBC), and platelets. An average-sized human being has a mixture of about 45 percent solid blood cells and 55 percent plasma. Blood flow patterns and blood vessels are consequential health risk factors and considerable contribution to morbidity and mortality so researchers, engineers, physiologists, and clinical persons focused serious attention on the study of blood flow in arteries. In terms of hematology, is at the forefront of numerous developments in the treatment or prevention of blood ailments. As a result, blood flow analysis is highly used in the hematology sector. The Finite Element Method (FEM) is used to investigate the flow in a three-dimensional computer model of a human aortic arch with three major branches to examine pulsatile blood flow concerning time. As a result of these concerns, people are rethinking and shifting their focus to fluid dynamics fields such as hematology, and magneto-hydro-dynamics (MHD).

Biomagnetic Fluid Dynamics (BFD) is comparatively a new area in fluid dynamics that studies the fluid flow in presence of a magnetic field. The interest regarding Biomagnetic fluids, specifically in bio-engineering and industry has extravagant significance due to the extensive implementations such as magnetic resonance imaging, magnetic drug targeting, magnetic devices for cell separation, adjusting blood flow during surgery, and transporting complex bio-waste fluids, controlling gastrointestinal disorders by the magnetic field, cancer tumor treatment, magnetic endoscopy, cell death by hyperthermia, power generation, aerodynamics heating, polymer technology, fluid droplet spray and so on. Since blood consists of a suspension of plasma and red blood cells (RBC) which contains hemoglobin. RBCs have hemoglobin fragments in high focus which are oxides of iron. Blood can be viewed as a suspension of the magnetic fragment in nonmagnetic plasma. The arc of the human aorta has been chosen for analyzing the flow pattern of non-Newtonian fluid as blood. Additionally, the volume of fluid (VOF) and pulsating wave velocity are

also added to both magnetic and non-magnetic effects to evaluate the difference between the blood velocity and pressures and wall shear stress.

1.1.1 Blood

Blood is a biological fluid that moves waste products of metabolism away from cells while delivering vital components such as nutrition and oxygen to them. Blood cells floating in blood plasma make up this substance. Plasma is primarily water (92 percent by volume) and contains dispersed proteins, carbohydrates, mineral ions, hormones, and blood cells themselves. Plasma makes up 55 percent of blood fluid. Red blood cells (also known as RBCs or erythrocytes) and white blood cells, such as leukocytes and platelets, make up the majority of blood cells.

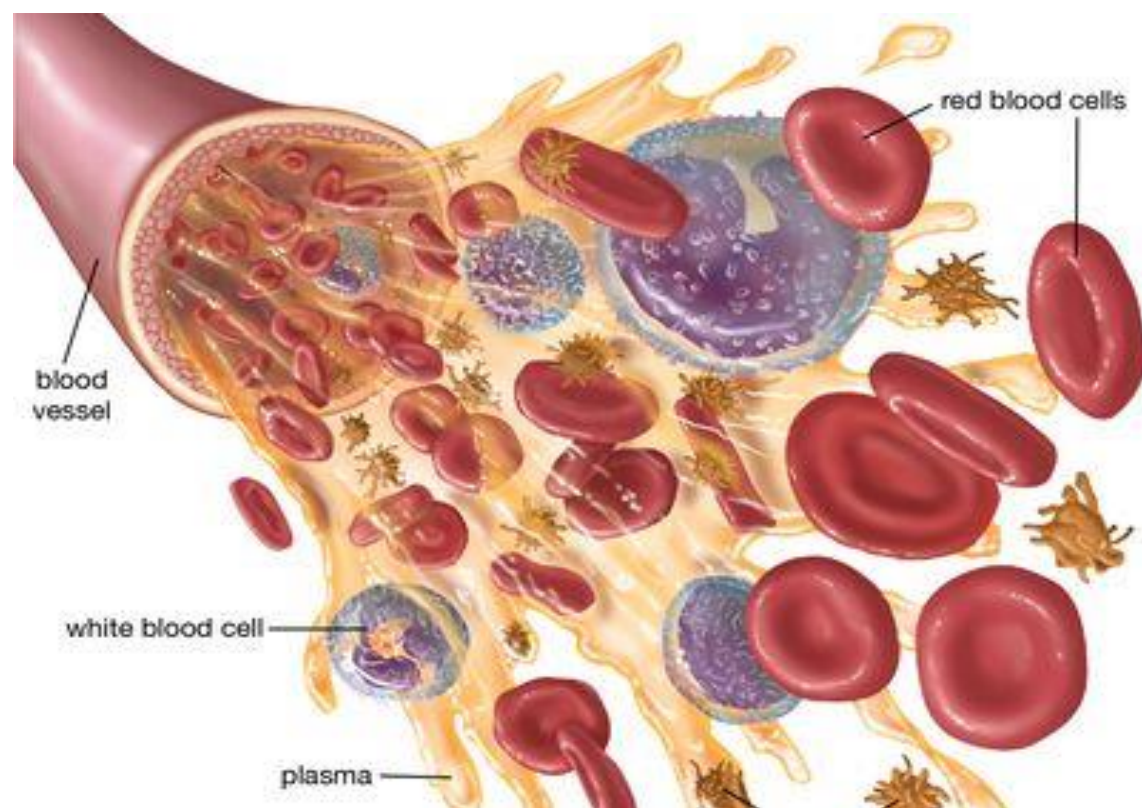


Fig. 1.1: Particles of blood

(<https://www.britannica.com/science/blood-biochemistry>) *Encyclopædia Britannica, Inc*

1.1.2 Plasma

Blood is always fluid within the body, and turbulent flow ensures that cells and plasma are mixed pretty evenly. Human blood volume varies depending on age, gender, weight, body type, and other factors, but an adult's blood volume is roughly 60 milliliters per kilogram of body weight. Per kilogram of body weight, a typical young male has a plasma volume of 35 milliliters and a red cell volume of 30 milliliters. The plasma, or liquid portion of the blood, is a complicated solution made up of more than 90% water. Plasma water is freely exchangeable with that of body cells and other extracellular fluids, allowing all tissues to maintain a normal level of hydration.

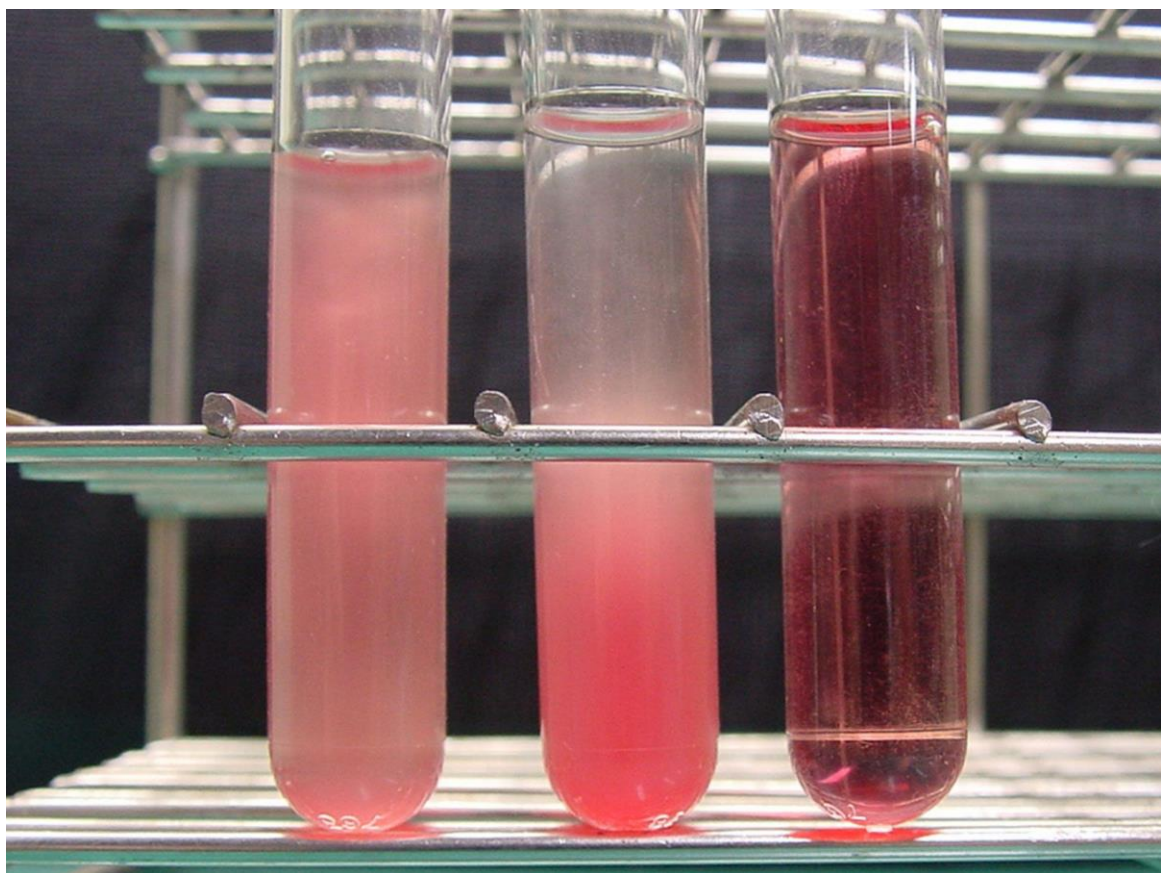


Fig. 1.2: Blood sediment in test tubes, showing plasma (left), red blood cells (middle), and the release of hemoglobin into the surrounding plasma (right)

© *Y tambe*

1.1.3 Blood Cells

Red blood cells (erythrocytes), platelets (thrombocytes), lymphocytes, and phagocytic cells are the four major types of blood cells. White blood cells are made up of lymphocytes and phagocytic cells together (leukocytes). Red blood cells absorb oxygen from the lungs and distribute it to the tissues; platelets help form blood clots; lymphocytes help with immunity, and phagocytic cells (granulocytes and monocytes) ingest and break down germs and foreign particles.

1.1.4 Red Blood Cell

Red blood cells are highly specialized and well-adapted to their principal job of delivering oxygen from the lungs to all bodily tissues. Red cells have a diameter of about 7.8 μm (1 μm = 0.000039 inches) and are shaped like biconcave disks, which have a large surface-to-volume ratio. Hemoglobin, the component responsible for oxygen delivery, makes up around 95% of the dry weight of a red blood cell. Hemoglobin is a protein that consists of four polypeptide chains (a tetramer), each with more than 140 amino acids. A heme group is a chemical structure that is bonded to each chain. Heme is made up of a ring-like chemical complex called porphyrin, which has an iron atom linked to it. As blood flows between the lungs and the tissues, it is the iron atom that binds oxygen reversibly. Each molecule of hemoglobin has four iron atoms, allowing it to bind four oxygen atoms. Under healthy settings, the complex porphyrin and protein structure provides the correct environment for the iron atom to bind and release oxygen appropriately. Hemoglobin has such a strong affinity for oxygen that at the oxygen pressure in the lungs, nearly 95% of the hemoglobin is saturated with oxygen. As the oxygen tension in the tissues diminishes, oxygen dissociates from hemoglobin and becomes available for diffusion across the red cell membrane and plasma to the places where it is needed.

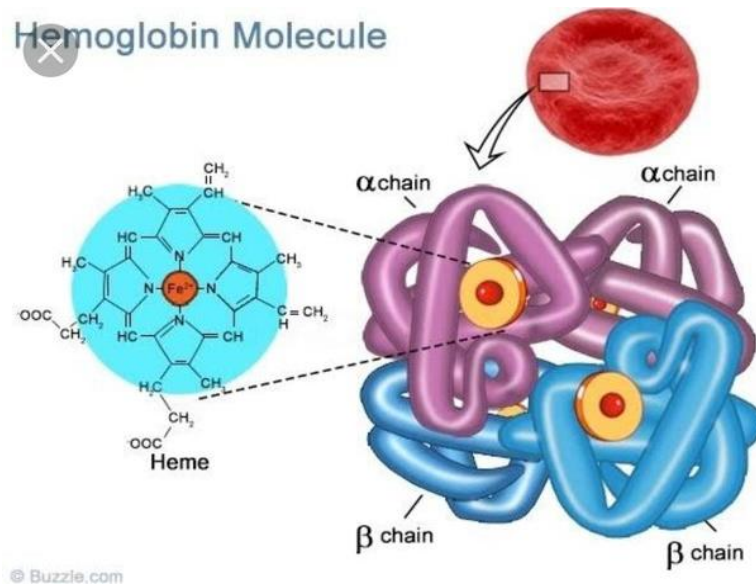


Fig. 1.3: Hemoglobin tetramer

(<https://timesofindia.indiatimes.com/blogs/antiaging/iron-metabolism-part-i-sources-transport-testing/>)

Two $\alpha\beta$ dimers combine to form the complete hemoglobin molecule. Each heme group contains a central iron atom, which is available to bind a molecule of oxygen. The $\alpha_1\beta_2$ region is the area where the α_1 subunit interacts with the β_2 subunit.

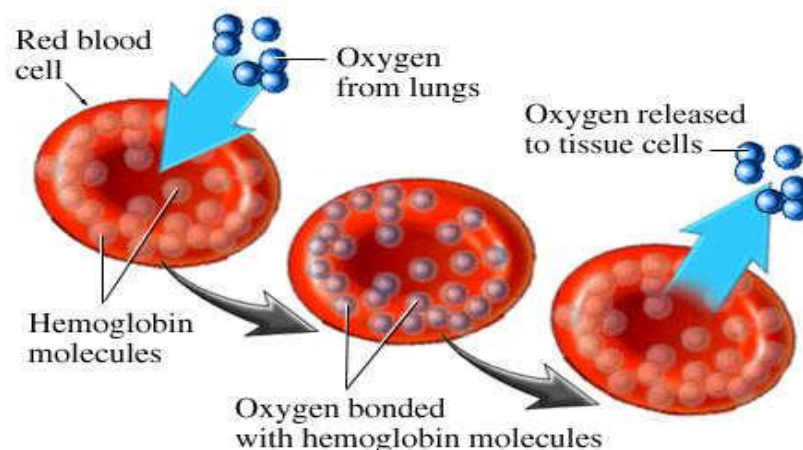


Fig. 1.4: Structure of hemoglobin

Hemoglobin's oxygen-carrying activity can be disrupted in a variety of ways. In both oxyhemoglobin and deoxyhemoglobin, the iron in hemoglobin is generally decreased or ferrous. Hemoglobin is converted to methemoglobin, a brown pigment incapable of transporting oxygen when the iron is oxidized to the ferric form. Although red blood cells include enzymes that keep iron in its normal state, aberrant situations can cause significant levels of methemoglobin to develop in the blood.

1.1.5 Heart

The human heart is mostly made up of a shell. Inside the heart, there are four cavities, or open areas, that fill with blood. The atria are two of these cavities. The other two organs are known as ventricles. The curving top of the heart is formed by the two atria. At the bottom of the heart, the ventricles come together to form a pointed base that points to the left side of your chest. Because the left ventricle contracts the hardest, we can feel our heart pumping most strongly on the left side of our chest. One atrium and one ventricle are located on the left side of the heart. The others are housed on the right side of the heart. The septum is a wall that separates the right and left sides of the heart. Each atrium is connected to the ventricle below it by a valve. The bicuspid valve is a valve that joins the left atrium and left ventricle. The right atrium and right ventricle are connected by the tricuspid valve. The semilunar valves allow blood to pass from the heart into the aorta and pulmonary artery, which are the two primary arteries. They obstruct blood flow back to the heart.

A few big blood arteries attach to the top of the heart. The aorta, or major artery, is the largest of them, carrying oxygen-rich blood away from the heart. The pulmonary artery, which connects the heart to the lungs as part of the pulmonary circulation system, is another significant arterial. Each atrium is connected to the ventricle below it by a valve. The bicuspid valve is a type of valve that is found in the heart. Because they are the "veins of the heart," they are called "vena cava."

Near the top of the heart, the superior is located. Underneath the superior is the inferior. The heart's design gives it a powerful, never-stopping pump. The heart pumps from the moment of conception to the moment of death. As a result, the heart must be strong. The cardiac muscle of the ordinary heart contracts and relaxes roughly 70 to 80 times each minute without you needing to think about it. Blood is pushed through the chambers and into the vessels as the heart muscle contracts. The speed with which the muscle contracts is controlled by nerves related to the heart.

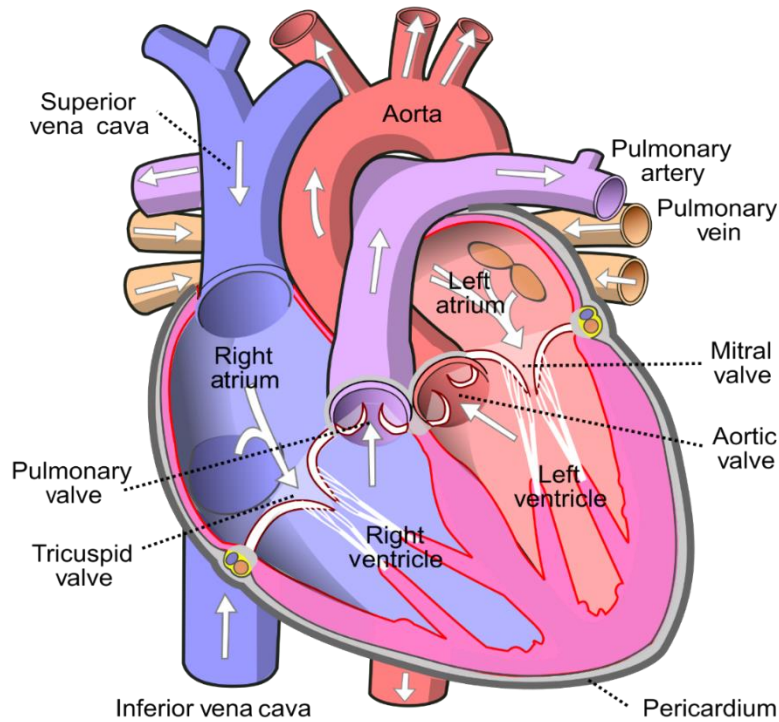


Fig. 1.5: Human heart

([https://en.wikipedia.org/wiki/File:Diagram_of_the_human_heart_\(cropped\).svg](https://en.wikipedia.org/wiki/File:Diagram_of_the_human_heart_(cropped).svg))

1.2 Objectives of the Thesis

Much research has already been done on the effect of pulsating velocity on arteries and stenosis arteries in the human body. But adding the VOF model and MHD effect in the aorta section is still a less focused zone. For this motive, a numerical investigation of the influence of MHD on the aorta section is considered for the present study, which includes the following:

- a) To use the pulsating blood flow model inside ascending aorta section in 3D for calculating velocity, temperature, pressure profile, and wall shear stress considering body temperature (310K).
- b) To Compare the blood flow without a magnetic field and under the influence of a magnetic field.

1.3 Scope of the Thesis

To perform the study, several scopes were considered, which are listed below:

- a) A 3D human aorta is designed to simulate the pulsating blood flow.
- b) Blood is modeled as Non-Newtonian fluid and the flow condition of working fluid is transient.
- c) As blood consists of plasma and solid particles like RBC, WBC, and protein. Therefore, multiphase flow is considered to model plasma and RBC.
- d) 1 Tesla MHD field is considered to determine the flow behavior of blood.
- e) RBC shows both paramagnetic and diamagnetic behavior. Oxygenated hemoglobin shows diamagnetism, a weak repulsion of the magnetic field while deoxygenated hemoglobin is paramagnetic, weakly attracted to the magnetic field which is beyond the scope of this study.
- f) The selected geometry is a smooth rigid body. The roughness and stenosis are not considered.

1.4 Structure of the Thesis

A brief discussion has been done for investigating the analysis of the arc of the human aorta having four circular outlet sections with and without the MHD is provided in this section:

In **Chapter One**, the prominence of this research work and how the study of fluid dynamics becomes one of the prominent resources for predicting blood behavior is discussed. Some general ideas of the present study, including the objectives of the thesis, are also mentioned.

In **Chapter Two**, the literature review and background of hematology are described. The development of fluid dynamics from the ancient period to the modern age is mentioned. The publications correlated with this present study and references are also included.

In **Chapter Three**, the conventional theories, like Euler's theory and the Navier-stokes theory, together with Maxwell and Lorentz's theory, are described. The theories that are correlated with this present work are taken into consideration. The effect of MHD on the flow is also mentioned.

In **Chapter Four**, a detailed computational methodology and governing equations, the design and fabrication of aorta, boundary conditions, selection of materials, and grid-cell independency test have been discussed.

In **Chapter Five**, a detailed illustration of the simulation procedure of the study is addressed. Validation, pulsating velocity profile, comparison of velocity, pressure, mass flow, and wall shear stress have been presented.

In **Chapter Six**, the conclusion of the present study, findings, and its limitations, along with the recommendation for future work, have been included.

CHAPTER 2

LITERATURE REVIEW

2.1 General

Arteriosclerosis is a frequent condition that has a significant impact on human health. It is the constriction of an artery in a specific location. Early arteriosclerotic injuries are not evenly distributed throughout the arterial tree; they tend to originate and grow in specific areas, such as the aorta proximal to the abdominal aorta, coronary arteries, and carotid bifurcations. It reduces blood flow to the organs and tissues of the body over time, posing significant health risks. The formation of fatty plaques, cholesterol, and other particles in and on the arterial walls generates artery stenosis. Smoking, a poor diet, or a variety of genetic factors can all cause it. Coronary artery disease (CAD) and stroke are caused primarily by atherosclerosis, which has various hereditary and environmental causes. hemodynamic variables (such as wall shear stress, static pressure, and so on) have been found to have an important role in the start and localization of arteriosclerosis.

Blood flow prediction is already in high demand in the biomedical industry and among specialists in various disciplines. For years, the hemodynamics of the cardiovascular system have been studied, and numerical simulations have helped us comprehend the low behavior in isolated stenotic arteries. Essentially, blood is pumped by the heart, which is covered and connected by a network of branching tubes, which suckers the blood from the heart and the blood artery distributes blood to various organs with nutrition. Blood is transported through two types of vessels: arteries and veins. Due to certain diseases, numerous investigations and studies have been conducted and are currently being conducted to determine the importance and impact of mechanical factors such as wall shear stresses, pressure and velocity gradients, and resistance to blood flow in atherosclerosis pathogens, as well as to locate and find the reasons for the onset and progression of atherosclerotic lesions. As a result of this, various studies have established a link between physiological and mechanical variables, with an initial focus on wall shear stress.

Many studies have been conducted in this area. The flow visualization techniques used in the early study on the physics of atherosclerosis were primarily experimental. Many of these trials yielded useful results. Other visualization techniques, such as dye tracing, provided additional insights on flow recirculation and flow separation. However, probing

the entire flow zone was not practicable. The recent usage of laser Doppler anemometry has allowed for more exact flow velocities to be acquired, as well as highly informative visualizations of flow behavior. Even the most advanced experimental techniques are used to obtain poor observations near the wall for some flow parameters, such as wall shear stress. Computer simulations have recently been praised as an effective tool for understanding flow within arteries. In comparison to experimental methods, computational simulations offer the benefit of being cost-effective. These simulations can provide medical practitioners with nearly any information that desire, such as flow velocities, pressures, and wall shear stresses. The volume of blood moving through the artery to deliver necessary nutrients is determined by blood flow velocity. Variations in artery geometry can interrupt the flow path, resulting in regions receiving fewer nutrients or life-sustaining elements. On the other hand, it would have the potential to promote the accumulation of hazardous compounds. As a result, understanding blood flow velocities is crucial to comprehending flow dynamics. The resistance to arterial flow is determined by the pressure within the artery. Forward flow is aided by a significant pressure drop across the artery. WSS on vessel walls has been difficult to quantify precisely and several times in the lab, but it has a strong link with arterial development. As a result, it is preferable to use computational simulations to obtain precise results. For evaluating the behavior of blood in arteries, computer-aided simulations are superior. They are capable of displaying fluid and solid behavior in a complete and exact manner. This can be simply deciphered and compared to the existing experimental data.

2.2 Early Studies of Blood Flow

From ancient times, researchers have been studying the fluid dynamical behavior of blood flow through a confined conduit. Lee and Fung (1970) performed an early numerical simulation of blood flow in an artery in which flow is observed in a typical constricted tube with a modest Reynolds number range of 0-25. A Gaussian normal distribution curve was utilized to specify a bell-shaped constriction. Oberkampf and Goh (1974) conducted similar numerical analyses. Lee and Fung employed an outflow-type boundary condition, but Oberkampf and Goh used an infinity condition. Atherosclerosis is a condition of the major arteries that manifests itself in areas of curvature and artery brunching. These are vulnerable areas for the formation and progression of atherosclerosis. Atherosclerotic anatomy is frequently linked to aberrant flow dynamics and stress distributions. According to Terbell (2003), atherosclerosis is more likely to develop in low-shear-stress areas, and fluctuating

shear stress enhances the risk of localization. With its curvature, branching, and distal tapering, the human aorta has a complex architecture. Because of the aorta's complicated structure, Gao et al. (2003) and Mori et al. (2002) discovered that the human aorta is prone to atherosclerosis localization. Blood flow in aorta models has also been numerically investigated by Kim et al. (2004), Morris et al. (2005), Nakamura et al. (2006), Park et al. (2007), and Shahcheranhi et al. (2002). Towfiq et al. (1986) and Dabagh et al. (2008) have shown that with a change in aorta size, the blood pressure is changing.

2.3 Review of Bio-magnetic Fluid Dynamics

BFD (Bio-magnetic Fluid Dynamics) is a relatively recent branch of fluid dynamics that studies fluid flow in the presence of a magnetic field. According to Hu, Meng, and Mandal (2005), magnetic drug targeting, magnetic devices for cell separation, changing blood flow during surgery, carrying complex bio-waste fluids, controlling gastrointestinal problems with the magnetic field, cancer tumor treatment, magnetic endoscopy, and cell death by hyperthermia are some of the key applications of bio-magnetic fluids, specifically in bio-engineering. Hemelrijck et al. (2018) and Ikehata et al. (2006) presented a detailed analysis of the utilization of magnetic fields in biological systems. RBC, WBC, platelets, and other particles are suspended in watery fluids like plasma to form human blood. RBCs have a high concentration of hemoglobin fragments, which are iron oxides. Blood can be thought of as a magnetic piece suspended in nonmagnetic plasma. The level of oxygenation determines the magnetic character of blood. Human blood is non-Newtonian by nature, but many researchers have studied blood flow in arteries and discovered that when blood moves through larger arteries at higher shear stress, it behaves in a Newtonian manner, whereas when blood moves through smaller arteries at lower shear stress, it behaves in a non-Newtonian manner. Rashidi et al. (2017), Tabakova et al. (2017), and Hammoud et al. (2019) explore how blood can behave as a non-Newtonian fluid in specific scenarios. However, some work such as Khanfar et al. (2006) showed that the non-Newtonian assumption of blood affects the blood flow in aorta aneurysms but in terms of shear stress calculation Newtonian and non-Newtonian simulation did not show any significant difference.

The magnetohydrodynamic flow of non-Newtonian fluids already has too much importance in bioengineering. Magnetic resonance imaging (MRI), heatstroke, and cancer therapy all benefit from such flow characteristics which are addressed by Tse et al. (2010), Das et al. (2013), and Sankar et al. (2011). Since blood is considered an MHD fluid, it helps to

manage blood pressure and is likely to be used to treat heart and vein infections. Using a magnetohydrodynamic methodology, Barnothy and Sumegi (1969) discovered that the use of an external magnetic field affects the organic frameworks. With a long-wavelength approximation, Mekheimer (2004) addresses blood flow in non-uniform channels under the influence of a magnetic field at zero Reynolds number. Halder and Ghosh (1994) focused on the effect of an externally imposed homogenous magnetic field on the quality of blood flowing through a single constricted blood artery in the heart.

One of the most challenging topics in fluid dynamics and biophysics is blood circulation in multi stenosis arteries impacted by the pulsatile pressure gradient. Hatami¹, Hatami² and Ganji (2014) research looked at blood as a third-grade non-Newtonian fluid transporting gold nanoparticles through a hollow porous tube, and it was discovered that a drop in the velocity profile correlates to an increase in the magnitude of the MHD parameter. Amlimohamadi, Akram, and Sadeghy (2016) investigated the transient fluid dynamic equations of blood flow through stenosis geometry, taking into account the non-Newtonian viscosity of blood as well as both magnetization and Lorentz forces. They looked at the true heart rate, intake velocity changes throughout time, and the effect of the magnetic field on different cardiac cycles.

Tzirtzilakis (2005) looked into a mathematical model for blood flow in a magnetic field. Mekheimer (2004) studied the effect of a uniform magnetic field on the peristaltic blood flow model by the concepts of magnetohydrodynamics, ferrohydrodynamics, and electrical conductivity. Jain, Sharma, and Singh (2009) present a mathematical model of blood flow in narrow and stenosis arteries under the effect of the magnetic field. Varshney Katiyar and Kumar (2010) investigate the numerical research of blood flow in a stenosis tube due to a magnetic field. Mekheimer et al. (2016) and Elnaqeeb et al. (2019) studies looked at blood flow models in stenosis arteries. Sharma, Singh, and Katiyar (2015) describe the effect of a magnetic field on blood parameters in the presence of magnetic particles through a circular tube. Zafar, Shah, and Khan (2019) investigated two-phase blood flow through a circular tube having magnetic characteristics. He discovered a comparison of the classical model's analytical and semi-analytical answers. Shah, Vieru, and Fetecau (2016) discovered the exact solutions to the blood flow model with fractional derivatives and magnetic nanoparticles in the cylindrical domain.

Numerous research on curved vessels has been conducted to determine the effect of vessel curvature, Reynolds number, Dean number, and Womersley number on the flow pattern by

Shahcheraghi et al. (2002). One of the most complicated flow scenarios in the cardiovascular system is blood flow via the aorta. Strong curvature effects, uneven geometry, tapering, and branching all contribute to this. These are sites for atherosclerotic lesions because of the abnormalities observed in the circulatory system, such as curvature, branching, and bifurcations which are studied by Weydahl and Moore (2001). The dependence on vessel geometries has been demonstrated in previous computer investigations. Papaharilaou, Doorly, and Sherwin (2002) demonstrated that out-of-plane coronary artery curvature models cause a bulk rotation of the velocity profile, resulting in Dean-type flow. Dean-like secondary flow characteristics in the right coronary artery were also extremely sensitive to local curvature effects, according to Myers et al. (2001). Different reconstruction approaches can thus significantly affect flow patterns, as Berthier, Bouzerar, and Legallais (2002) discovered computationally while modeling the impact of different reconstruction methods for coronary arteries. Previous CT or MRI-based numerical models of the human aorta, which incorporated the aortic arch, had several model simplifications. Approximating the cross-sections as circles Shahcheragi et al. (2002) adopts a constant diameter throughout the model and Mori and Yamaguchi (2002) are examples of such simplifications. The current research involves a numerical evaluation of unstable and steady blood flow using various reconstruction methods of a human aortic arch and derived from spiral CT images. The goal of this research was to see how adding model simplifications affected the flow regime.

2.4 This Work

This study is motivated by previous studies and seeks to imitate pulsing blood flow via human arteries in predicting fluid flow. The numerical study of a three-dimensional and pulsatile blood flow in a human aortic arch and its three principal branches. Several simulations incorporating Non-Newtonian blood flow, magnetic effect, and VOF model through each artery have been conducted separately. However, little research has been done on combining all of the above circumstances. This research seeks to analyze the flow characteristics of Non-Newtonian pulsatile flow with VOF (plasma and RBC) through arteries, as well as the magnetic influence.

CHAPTER 3

Related Theories

3.1 Continuity Equation

The fundamental continuity equation is a formula that describes how intensive property changes over time. An intense property is unaffected by the amount of material available. Temperature, for example, is an intensive attribute, while heat is a comparable extensive property. The obtained continuity equation can be applied to mass and momentum later. The continuity equation, often known as the conservation of mass equation, states that the fluid mass cannot be altered. That is the flow may be steady or unsteady, viscous or frictionless, compressible or incompressible.

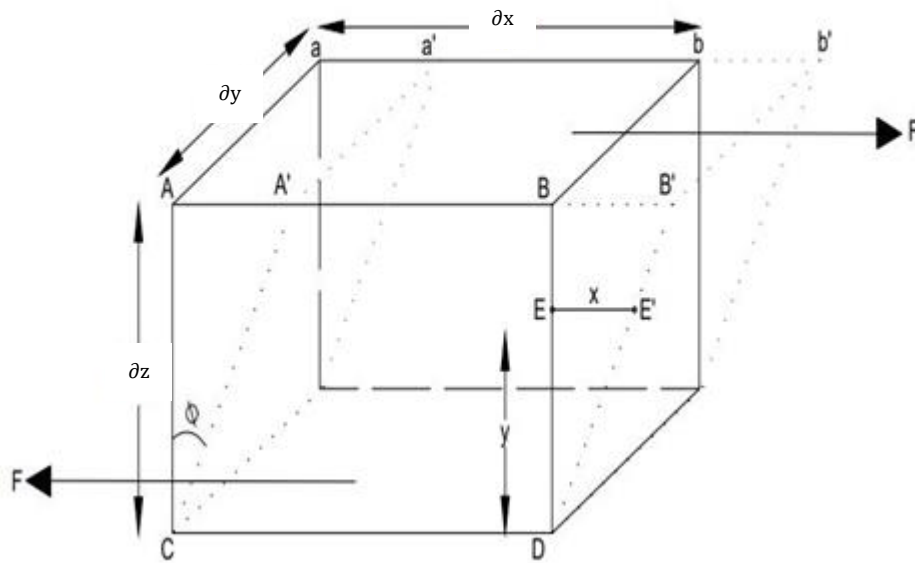


Fig. 3.1: Control volume.

$$\frac{\partial \rho}{\partial t} + \frac{\partial}{\partial x}(\rho u) + \frac{\partial}{\partial y}(\rho v) + \frac{\partial}{\partial z}(\rho w) = 0 \quad (3.1)$$

Or,

$$\frac{\partial \rho}{\partial t} + \nabla \cdot (\rho V) = 0 \quad (3.2)$$

If the flow is steady, then the equation be $\nabla \cdot (\rho V) = 0$;

If the flow is incompressible then the equation be $\nabla \cdot V = 0$

3.2 Navier-Stokes Equation

The Navier-Stokes equations are a set of partial differential equations that explain the motion of viscous liquids. They're called after the French engineer and physicist Claude-Louis Navier and Anglo-Irish physicist and mathematician George Gabriel Stokes. In Newtonian fluids, the Navier–Stokes equations express momentum and mass conservation quantitatively. A state equation is usually used to relate pressure, temperature, and density.

Considering body force and unsteady state:

In x-direction,

$$\frac{\partial u}{\partial t} + u \frac{\partial u}{\partial x} + v \frac{\partial u}{\partial y} + w \frac{\partial u}{\partial z} = -\frac{1}{\rho} \frac{\partial p}{\partial x} + \mathcal{V} \left(\frac{\partial^2 u}{\partial x^2} + \frac{\partial^2 u}{\partial y^2} + \frac{\partial^2 u}{\partial z^2} \right) - g \frac{\partial h}{\partial x} \quad (3.3)$$

In y-direction,

$$\frac{dv}{dt} + u \frac{dv}{dx} + v \frac{dv}{dy} + w \frac{dv}{dz} = -\frac{1}{\rho} \frac{dp}{dy} + \mathcal{V} \left(\frac{d^2v}{dx^2} + \frac{d^2v}{dy^2} + \frac{d^2v}{dz^2} \right) - g \frac{dh}{dy} \quad (3.4)$$

In z-direction,

$$\frac{dw}{dt} + u \frac{dw}{dx} + v \frac{dw}{dy} + w \frac{dw}{dz} = -\frac{1}{\rho} \frac{dp}{dz} + \mathcal{V} \left(\frac{d^2w}{dx^2} + \frac{d^2w}{dy^2} + \frac{d^2w}{dz^2} \right) - g \frac{dh}{dz} \quad (3.5)$$

Those are Navier-stokes equations in cartesian coordinates.

In vector form,

$$\underbrace{\rho \left(\frac{d\vec{v}}{dt} + \vec{V} \cdot \nabla \vec{V} \right)}_{\text{Acceleration term}} = \underbrace{-\nabla p}_{\text{Volumetric force + gravity}} + \underbrace{\mu \nabla^2 \vec{v}}_{\text{viscosity}} + \underbrace{\sum \vec{f}}_{\text{gravity}} \quad (3.6)$$

Navier-stokes equation can explain incompressible Newtonian fluid in daily life like water, and air (subsonic speed). Basically, Navier-stokes equation is a sophisticated form of Newton's 2nd law and it deals with volumetric forces.

3.3 Viscosity

The most essential fluid property in the research of fluid flow is viscosity. The characteristic of a fluid's viscosity is its resistance to shear operating on it. To put it another way, viscosity is a measurement of a fluid's resistance to flow. In more detail, it estimates the fluid strain rate generated by particular applied shear stress.

Consider a fluid facing shear stress \mathcal{T} , as in Figure 3.2. As long as the shear stress \mathcal{T} is maintained, the shear strain angle $\Phi=\delta\theta$ will grow with time continuously. The upper surface of this element is moving at a higher speed than the lower surface of this element. such fluid shows a linear relationship between shear stress and strain rate.

According to Newton's law of viscosity,

Shear stress \propto rate of strain

$$\mathcal{T} \propto \frac{\delta\theta}{\delta t}$$
$$\mathcal{T} = \mu \frac{\delta\theta}{\delta t} \quad (3.7)$$

Where, μ =constant viscosity of the fluid

The kinematic viscosity or momentum diffusivity is the ratio of the dynamic viscosity μ to the density of the fluid ρ . It is usually denoted by the Greek letter nu (ν). That is,

$$\nu = \frac{\mu}{\rho} \quad (3.8)$$

Viscosity is typically designated in units of centipoise or poise but can be expressed in other acceptable measurements as well. Some conversion factors are as follows:

$$100 \text{ Centipoise} = 1 \text{ Poise}$$

$$1 \text{ Centipoise} = 1 \text{ mPa s (Millipascal Second)}$$

$$1 \text{ Poise} = 0.1 \text{ Pa s (Pascal Second)}$$

3.4 Newtonian and Non-Newtonian Fluid

The fluid which follows Newton's law of viscosity (3.7) is known as Newtonian fluid whereas the fluid that does not act on the equation is known as Non-Newtonian fluid. A Newtonian fluid is one in which the viscous stresses generated by its flow are directly proportional to the current strain rate, the rate at which its deformation changes over time at every place. The simplest mathematical models of fluids that account for viscosity are

Newtonian fluids. Water and air can be assumed as Newtonian fluids under specific conditions.

A non-Newtonian fluid is one whose flow properties differ from those of Newtonian fluids in some way. Most Non-Newtonian fluids' viscosity (the ability of a fluid to withstand progressive deformation by shear or tensile stresses) is determined by shear rate or shear rate history. Normal stress differences or other Non-Newtonian behavior can still be seen in some Non-Newtonian fluids with shear-independent viscosity. Many salt solutions and molten polymers, as well as many commonly found compounds like ketchup, custard, toothpaste, starch suspensions, paint, blood, and shampoo, are Non-Newtonian fluids. In a Newtonian fluid, the relationship between shear stress and shear rate is linear, passing through the origin, with the coefficient of viscosity as the proportionality constant. The relationship between shear stress and shear rate in a Non-Newtonian fluid is different and can even be time-dependent (Time-Dependent Viscosity). As a result, a constant viscosity coefficient cannot be determined.

Table 3.1: Examples of Newtonian and non-Newtonian fluid

Newtonian fluid	Non-Newtonian fluid (time-independent)		Non-Newtonian fluid (time-dependent)	
	Dilatant	Pseudoplastic	Thixotropic	Rheopectic
Water	Quicksand	Ketchup	Drilling mud	Gypsum paste
Air	Corn flour	Polymer solution	Paints	Cream
Gasoline	Starch in water	Greases	Asphalt	Bentonite clay
Alcohol	Potassium silicate in water	Detergent slurries	Glue	Printer ink

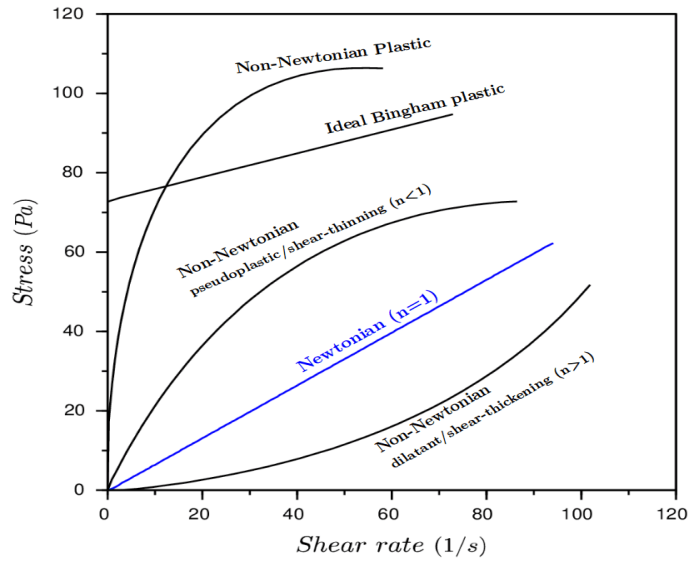


Fig. 3.2: Stress vs strain curve of Newtonian and non-Newtonian material.
<https://www.simscale.com/docs/simulation-setup/materials/non-newtonian-models/>

Blood is a non-Newtonian, shear-thinning fluid with thixotropic and viscoelastic properties. Many cardiovascular handbooks consider blood viscosity values between 3.5 and 5.5 cP. In the Navier Stokes equation (3.6), viscosity is fixed. If we can define that viscosity is changing and incorporate it in the Navier Stokes equation (3.6), it will predict the Newtonian behavior of a fluid. When measuring the flow of fluids such as liquids, semi-solids, gases, and even solids, viscosity is an important factor to consider. Anyone working in flow measurement, whether in research and development, quality control, or fluid transfer, will find some form of viscosity measurement at some point. Viscosity measurement models include the following:

- a. Power-law model,
- b. Carreau model,
- c. Generalized Power Law or Ballyk model,
- d. Cross model, and so on.

Fuchs and Alexander (2020) found no significant difference for these models on arteries simulation. Gerasim and Krivovichev (2021) compared one-dimensional hemodynamic structures with different models and suggested that NNFs (non-Newtonian Factors) are better in the Carreau model.

3.5 Wall Shear Stress

Under the "no-slip" condition put on the boundary, fluid in contact with the vessel wall will travel at the same velocity as the wall. For theoretical validation, time average wall shear stress (TAWSS) can be calculated.

$$\text{TAWSS} = \frac{1}{T} \int_0^T |wss(s, t)| dt \quad (3.9)$$

3.6 Magneto-Hydro-Dynamics (MHD)

The study of the magnetic characteristics and behavior of electrically conducting fluids is known as magnetohydrodynamics (MHD; also known as magneto-fluid dynamics or hydro-magnetics). Plasmas, liquid metals, salt water, and electrolytes are examples of magneto fluids. The term "magneto-hydro-dynamics" comes from the words magneto, which means magnetic field, hydro, which means water, and dynamics, which means movement. The basic idea behind MHD is that magnetic fields can induce currents in a flowing conductive fluid, polarizing the fluid and changing the magnetic field reciprocally. MHD is described by a set of equations that combines the Navier–Stokes equations for fluid dynamics and Maxwell's equations for electromagnetism.

3.6.1 Maxwell Equation

Maxwell's equations are a set of coupled partial differential equations that constitute the foundation of classical electromagnetism, classical optics, and electric circuits, together with the Lorentz force law. They explain how charges, currents, and changes in the fields generate electric and magnetic fields.

3.6.1.1 Gauss Law of Electrostatics

The relationship between a static electric field and electric charges are described by the Gauss law: a static electric field points away from positive charges and toward negative charges, and the net outflow of the electric field through a closed surface is proportional to the enclosed charge, including bound charge due to material polarization. The permittivity of free space is the proportion's coefficient.

$$\nabla \cdot \vec{E} = \frac{\rho_c}{\epsilon_0} \quad (3.10)$$

3.6.1.2 Gauss Law of Magnetism

According to the Gauss law of magnetism, electric charges have no magnetic equivalents, which are referred to as magnetic monopoles. Instead, a material's magnetic field is attributed to a dipole, and the magnetic field's net outflow through a closed surface is zero. Magnetic dipoles can be thought of as current loops or inseparable pairs of equal and opposite magnetic charges.' In a Gaussian surface, the total magnetic flux is zero, and the magnetic field is a solenoidal vector field.

$$\nabla \cdot \vec{B} = 0 \quad (3.11)$$

This is similar to our continuity equation in fluid, $\nabla \cdot u = 0$ (3.12)

3.6.1.3 Faraday Law

Faraday's law of induction is an electromagnetism fundamental law that predicts how a magnetic field interacts with an electric circuit to produce an electromotive force (emf), a process known as electromagnetic induction. In simple terms, time changing magnetic field can create an electric field.

$$\nabla \times \vec{E} = -\frac{d\vec{B}}{dt} \quad (3.13)$$

Which is similar to the vorticity in fluid, $\vec{\omega} = \nabla \times \vec{v}$ (3.14)

3.6.1.4 Ampere-Maxwell Law

An electric current and an electric field that changes with time create a circulating magnetic field. This equation is capable of generating electromagnetic waves.

$$\nabla \times \vec{B} = \mu_0 \vec{j} + \frac{1}{c^2} \frac{d\vec{E}}{dt} \quad (3.15)$$

Where, $\vec{j} = \rho_c \vec{V}$ (3.16)

This velocity \vec{V} happens to be as same as fluid velocity.

Together this four (3.10), (3.11), (3.13), and (3.15) equations create electromagnetic phenomena.

3.6.2 Lorentz' Force

The Lorentz force (or electromagnetic force) is the result of electromagnetic fields combining electric and magnetic forces on a point charge. The electromagnetic force on a

charge q is described as a combination of a force in the direction of the electric field E , proportional to the magnitude of the field and the quantity of charge, and a force at right angles to the magnetic field B and the charge's velocity v , proportional to the magnitude of the field, the charge, and the velocity.

$$\vec{F} = q\vec{E} + q\vec{V} \times \vec{B} \quad (3.17)$$

3.6.2.1 Volumetric Lorentz' Force

$$\frac{\vec{F}}{V_0} = \frac{q}{V_0}\vec{E} + \frac{q}{V_0}\vec{V} \times \vec{B}$$

$$\text{Or,} \quad \vec{f} = \rho_c \vec{E} + \rho_c \vec{V} \times \vec{B}$$

$$\therefore \quad \vec{f} = \rho_c \vec{E} + \vec{J} \times \vec{B} \quad (3.18)$$

If we consider no electric field, then $\rho_c \vec{E} = 0$

From Navier-stokes equation (3.18),

$$\rho \frac{D\vec{V}}{Dt} = -\nabla\rho + \mu\nabla^2\vec{V} + \vec{f}$$

Substituting the value of gravitational force and Lorentz's force,

$$\rho \frac{D\vec{V}}{Dt} = -\nabla\rho + \mu\nabla^2\vec{V} + \vec{J} \times \vec{B} - g\nabla h \quad (3.19)$$

$$\text{Or,} \quad \rho \frac{D\vec{V}}{Dt} = -\nabla\rho + \mu\nabla^2\vec{V} + \rho_c \vec{V} \times \vec{B} - g\nabla h \quad (3.20)$$

[from equation (3.16)]

These two type \vec{V} happens through phenomena which are called freezing together of the fluid and magnetic fluid. So they are coupled in magnetic induction lines and fluid.

From equation (3.15), if $\frac{d\vec{E}}{dt} = 0$

$$\text{Then,} \quad \frac{\nabla \times \vec{B}}{\mu_0} = \vec{J}$$

So, equation (3.19) becomes,

$$\rho \frac{D\vec{V}}{Dt} = -\nabla\rho + \mu\nabla^2\vec{V} + \frac{\nabla \times \vec{B}}{\mu_0} \times \vec{B} - g\nabla h$$

$$\text{Or,} \quad \rho \frac{D\vec{V}}{Dt} = -\nabla\rho + \mu\nabla^2\vec{V} + \frac{(\nabla \cdot \vec{B})\vec{B}}{\mu_0} - \frac{\nabla B^2}{2\mu_0} - g\nabla h$$

$$\text{Or,} \quad \rho \frac{D\vec{V}}{Dt} = -\nabla\rho + \mu\nabla^2\vec{V} + \frac{(\nabla \cdot \vec{B})\vec{B}}{\mu_0} - \frac{\nabla B^2}{2\mu_0} - g\nabla h$$

$$\therefore \quad \rho \frac{D\vec{V}}{Dt} = \mu\nabla^2\vec{V} + -g\nabla h - \nabla\left(\rho + \frac{\nabla B^2}{2\mu_0}\right) + \frac{(\nabla \cdot \vec{B})\vec{B}}{\mu_0} \quad (3.21)$$

This is the combined equation of Navier-stokes and Maxwell's.

Physical terms: $\frac{\nabla B^2}{2\mu_0} = \textit{magnetic pressure}$

$$\frac{(\nabla \cdot \vec{B}) \vec{B}}{\mu_0} = \textit{magnetic tension}$$

CHAPTER 4

GOVERNING EQUATIONS AND COMPUTATIONAL ANALYSIS

4.1 Introduction

A computational study has been conducted to simulate the three-dimensional human aorta model with and without a magnetic field. The unsteady, viscous, three-dimensional governing equations are described in this chapter and solved by the multiphase VOF model. ANSYS Fluent 2020R1 software is used to simulate the stated problem.

4.2 Governing Equations

The primary three governing equations are conservation of mass, conservation of momentum, and conservation of energy. Additionally, there are auxiliary equations due to the velocity fluctuation over the entire domain. The differential equations for laminar flows are expressed as:

$$\begin{aligned}\frac{\partial \rho}{\partial t} + \frac{\partial}{\partial x}(\rho u) + \frac{\partial}{\partial y}(\rho v) + \frac{\partial}{\partial z}(\rho w) &= 0 \\ \frac{\partial \rho}{\partial t} + \frac{\partial}{\partial x_i}(\rho u_i) &= 0\end{aligned}\tag{4.1}$$

Navier-stokes and Maxwell equations are also applied,

$$\therefore \rho \frac{D\vec{V}}{Dt} = \mu \nabla^2 \vec{V} + -g \nabla h - \nabla \left(\rho + \frac{\nabla B^2}{2\mu_0} \right) + \frac{(\nabla \cdot \vec{B}) \vec{B}}{\mu_0}$$

4.3 Viscosity Modeling

From the various model of viscosity, the Carreau Yasuda model is used for blood flow analysis. It is an empirical equation used to fit non-Newtonian fluid.

$$\mu = \mu_\infty + (\mu_0 - \mu_\infty) [1 + (\gamma_C \dot{\gamma})^2]^{\frac{n-1}{2}}\tag{4.2}$$

Table 4.1: Properties for blood in Carreau model

Infinite shear viscosity, μ_∞	0.0035 kg/ms
Zero shear viscosity, μ_0	0.056 kg/ms
<i>Time constant, γ_c</i>	3.313 lambda(s)
Power law index, n	0.3568

4.4 Selection of Multiphase Modeling

Multiphase is a flow in which more phases coexist in the same flow domain. For example, gas bubbles in the liquid, a liquid droplet in gas, solid particles in gas or liquid, etc.

The available 7 models in this version of ANSYS Fluent are:

- a) Eulerian multiphase model (EMP)
- b) Mixture multiphase
- c) Volume of fluid (VOF)
- d) Dispersed multiphase
- e) Fluid film
- f) Lagrangian multiphase model (LMP)
- g) Discrete element method (DEM)

The selection of the appropriate multiphase model substantially affects the solution of the specific problems. Here, the VOF model is used to calculate the mixture of plasma and red blood cells with and without magnetic effect.

4.5 Computational Set-up

Computational simulations are performed using the ANSYS Fluent 2020R1 software assuming an unsteady, incompressible, and isothermal flow.

4.5.1 Human aorta section design

The chosen section of the human aorta is designed using SOLIDWORKS software. The ascending aorta, brachiocephalic artery, left common carotid artery, left subclavian artery, and descending aorta section is selected to investigate the blood flow by Florescu and Maria (2018). Starting with ascending aorta to descending aorta, the whole section is tapered.

Table 4.2: diameter of aorta section

Section name	Diameter (mm)
Ascending aorta	27.50
Brachiocephalic artery	8.80
Left common carotid artery	8.50
Left subclavian artery	9.90
Descending aorta	20.50

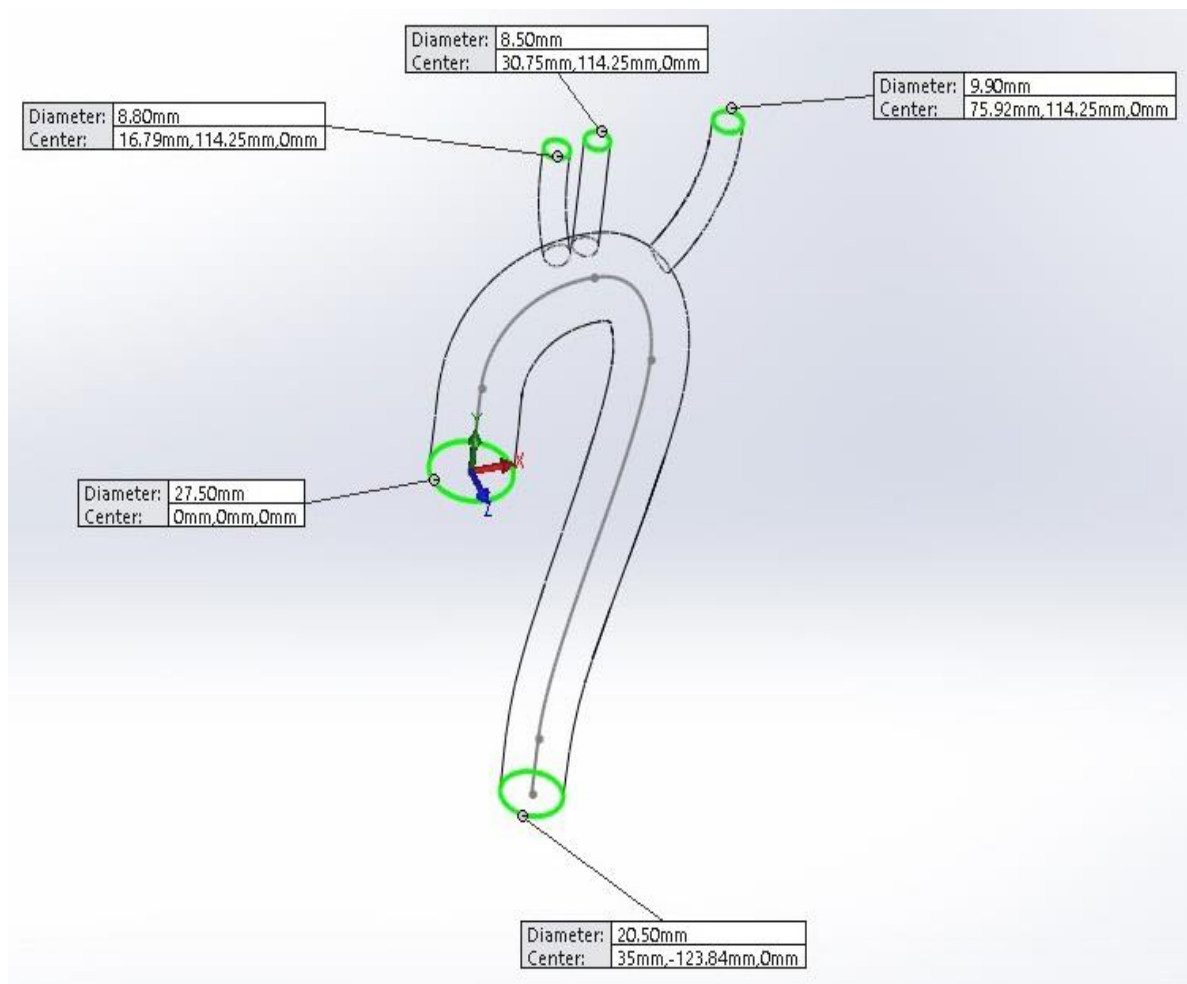


Fig. 4.1: A three-dimensional design with inlet and outlet diameter.

4.5.2 Computational Geometry and boundary conditions

A computational domain is required for 3D CFD analysis. The CFD analysis is done to determine the velocity profile, pressure, and wall shear stress due to the pulsating flow driving from the heart to the aorta with and without MHD.

A three-dimensional domain with four major branches as an outlet model is considered for simulations. The computational domain required for the analysis is shown in Fig. 4.2 with the necessary dimensions. The boundary conditions are very crucial for accurate simulation. A velocity inlet boundary condition is applied at the inlet section of the domain. A pressure outlet boundary condition is implemented at the outlet section of the domain. The surfaces are considered as walls with no-slip boundary conditions. The following boundary conditions are used in the model shown in Table 4.3.

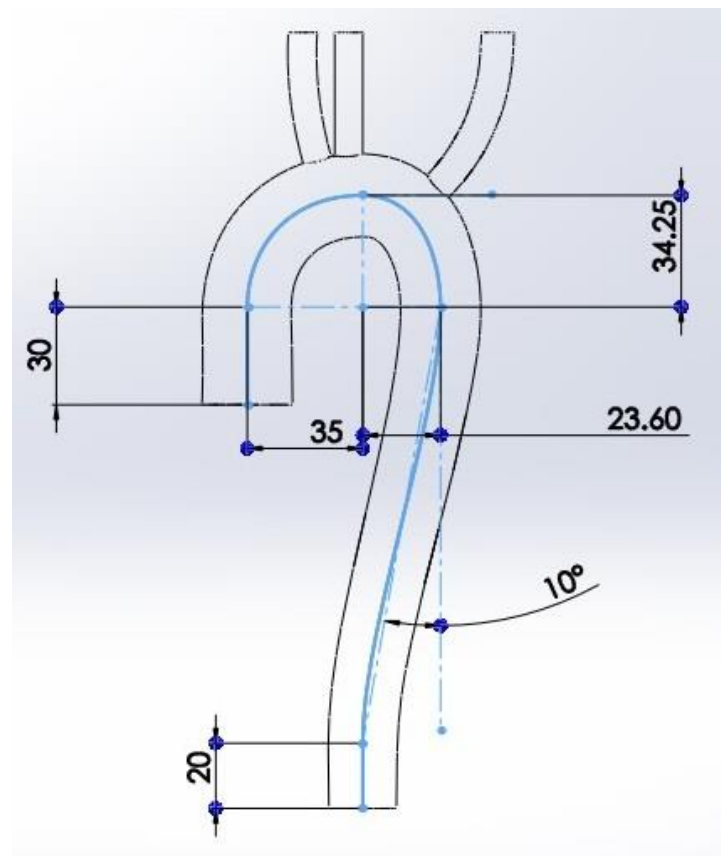


Fig. 4.2: Design of selected human arteries with dimension (two dimensional).



Fig. 4.3: Design of selected human arteries in isometric view.

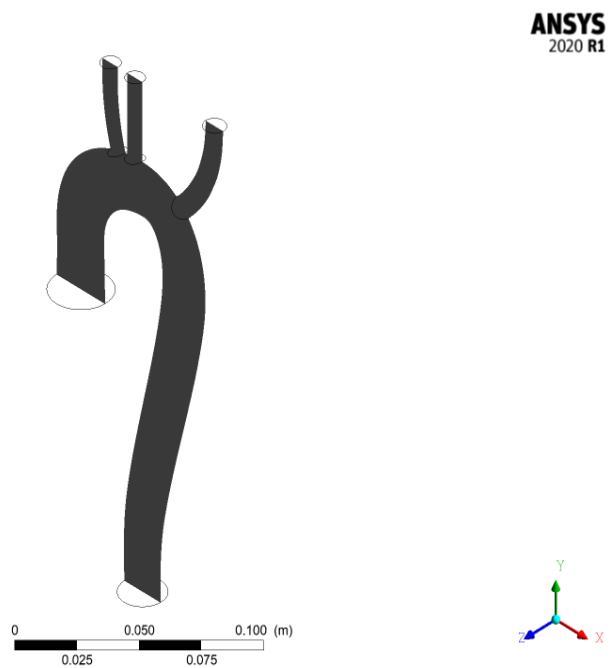


Fig. 4.4: A cross-sectional plane in xy direction.



Fig. 4.5: Three-dimensional meshing domain.

Table. 4.3: Boundary conditions

Domain	Boundary	Type
Blood Domain	Inlet	Velocity-Inlet
	BT outlet	Pressure-Outlet
	LS outlet	Pressure-Outlet
	LC outlet	Pressure-Outlet
	Outlet	Pressure-Outlet
	Wall	Wall

4.5.2.1 Boundary condition for inlet

Ascending aorta is the inlet section in this geometry. As the heart pumped blood in pulsating order. Blood flow enters the ascending aorta through a one-way valve. This pulsating entry is designed by a user-defined file (UDF) using C programming code. Sinn et al. (2005) used the following mathematical equation for the pulsating solution.

The mathematical equation used for the pulsating velocity inlet is given below.

$$v_{inlet} = \begin{cases} 0.5 \sin[4\pi(0.0160236 + t)] & ; 0.5n < x \leq 0.218 \\ 0.1 & ; 0.5n + 0.218 < n \leq 0.5(n + 1) \\ n = 0,1,2 \dots \dots \end{cases} \quad (4.5)$$

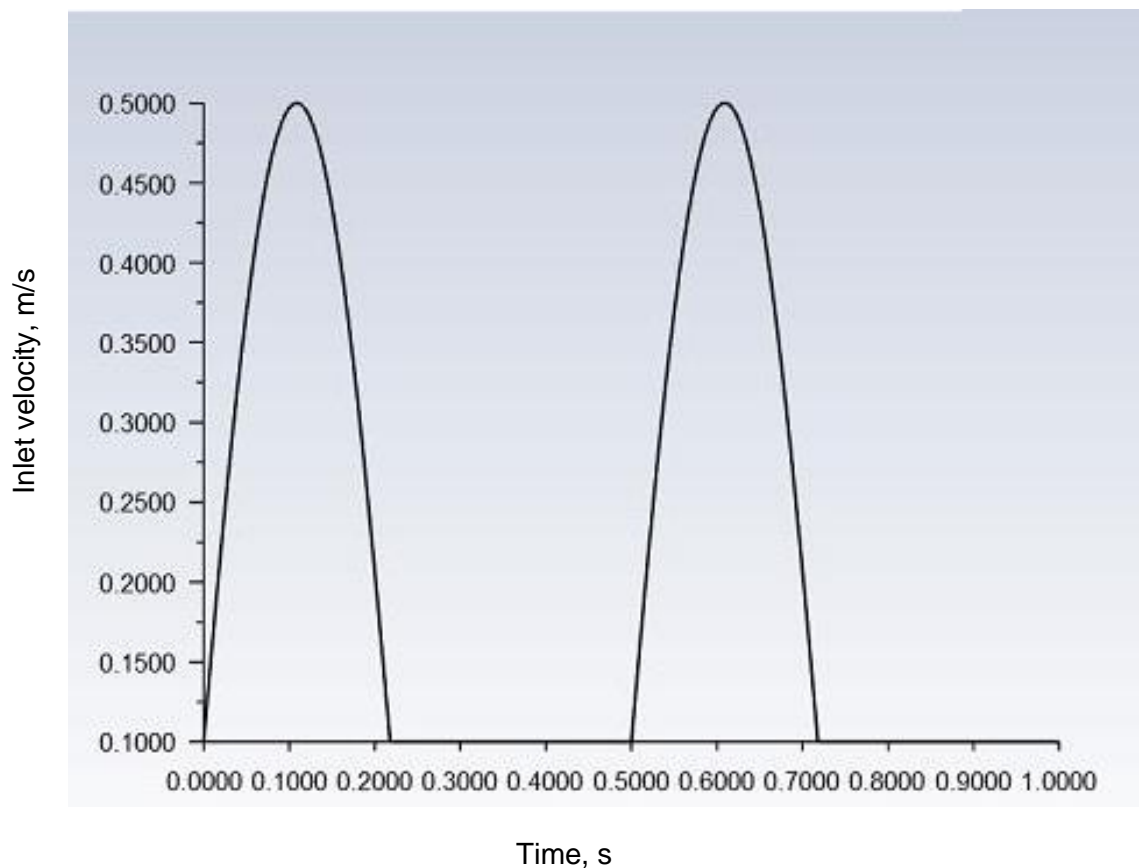


Fig. 4.6: Inlet velocity profile.

4.5.2.2 User defined function for inlet

The following code is used to generate a profile of pulsating velocity in the inlet section.

```
DEFINE_PROFILE(inlet_velocity,t,i)
{
    face_t f;
    begin_f_loop(f,th)
    double t = (CURRENT_TIME*2-floor(CURRENT_TIME*2))/2;
    //t is the local time within each period
    {
        if (t <= 0.218)
            F_PROFILE(f,t,i) = 0.5*sin(4*PI*(t+0.0160236));
        else
            F_PROFILE(f,th,i) = 0.1;
    }
    end_f_loop(f,t);
}
```

4.5.3 Parameters for Materials

In the multiphase model, we consider plasma and RBC mixture to determine the flow analysis of blood. Plasma is considered liquid and RBCs are considered semi-solid.

Table 4.4: Properties of materials

Phase 1	Plasma
Density (kg/m ³)	1003
Viscosity (Pa.s)	0.001
Phase 2	RBC
Density (kg/m ³)	1080
Viscosity (Pa.s)	Carreau-Yasuda

Two configurations, i.e., without and with magnetic field with the same setup, are designed and simulated.

4.5.4 Numerical Scheme

The numerical simulations are carried out using the well-known ANSYS Fluent 2020R1 program. The solver type is chosen to be a pressure-based approach. This solver is chosen for an incompressible fluid. In the blood flow, there is no heat transfer. For pressure-velocity coupling, the SIMPLE algorithm is used in solution approaches. The momentum equation is discretized using the Second Order Upwind method as a numerical scheme. With 1000 total time steps, the time step is set to 0.001 seconds. Each time step process is subjected to a maximum of 1000 iterations. Between two consecutive time steps, the time-stepping is determined by error estimation of all dependent variables. For all dependent variables time steps, the limiting convergence requirements of residual are set to $1e-6$.

Table 4.5: Overall system and solver requirement

Solver	Fluent
Material	Blood (as RBC) Water (as plasma)
Software use	ANSYS 2020R1
Post-processing	Contour plot (velocity, pressure, mass flow rate)
System requirement	Workstation (Core i7) RAM 32GB

4.5.5 Mesh Generation

Mesh generation has a significant impact on CFD solutions. Meshes used in computer simulations are often classified as either structured or unstructured meshes. Unstructured meshes are used for this research because they give better conformance to complicated geometries and consume less computing memory than structured meshes which is mentioned by Jonathan. (1997). The whole domain is discretized into several elements or

grid cells and unstructured mesh is generated having approximately tetrahedron grids of 2,101,155 and 327,780 nodes. The minimum cell size is 1×10^{-3} m. The maximum aspect ratio = $1.96295e+01:1$

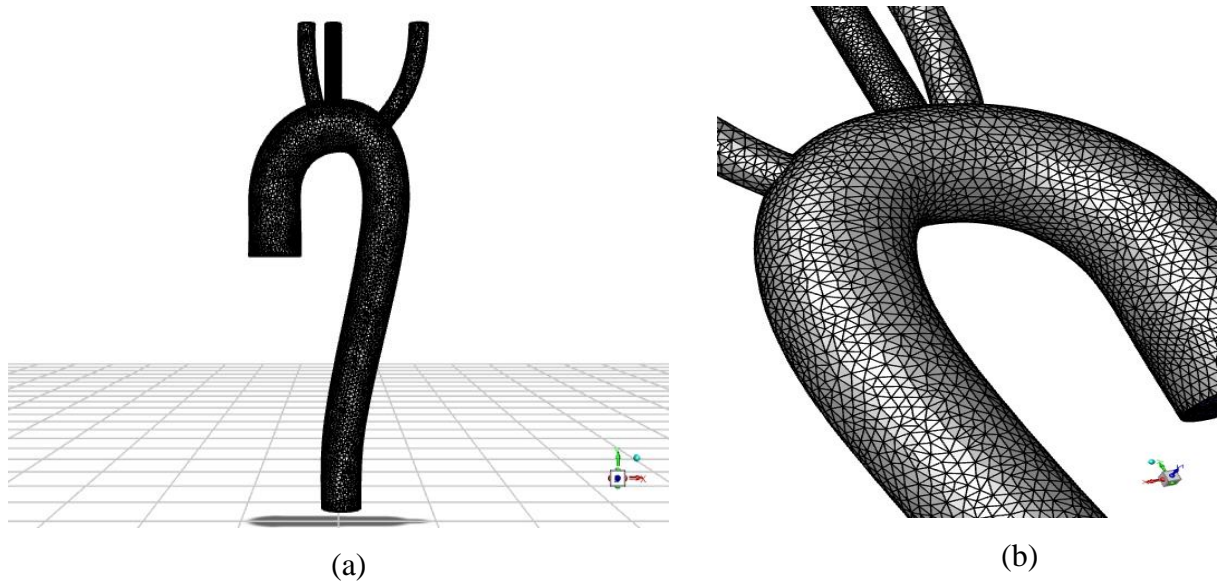


Fig. 4.7. a) Meshing view b) Close view of meshing around the arc.

4.6 Mesh Sensitivity Test

A Grid-independency test is performed to validate the computational results for the simulation of blood flow. The maximum velocity is selected as the factor of the judgment of the mesh validation test. To ensure the solution's independence, computational analysis is done for three different ranges of grid cells (i.e., from 2,101,155 to 50,000 no of elements). Figure 4.8 describes the results of the velocity vs mesh size. The figure shows that the output velocity values are getting similar from the initial mesh 3 to mesh 1. Finally, mesh 1 was used for the final calculation.

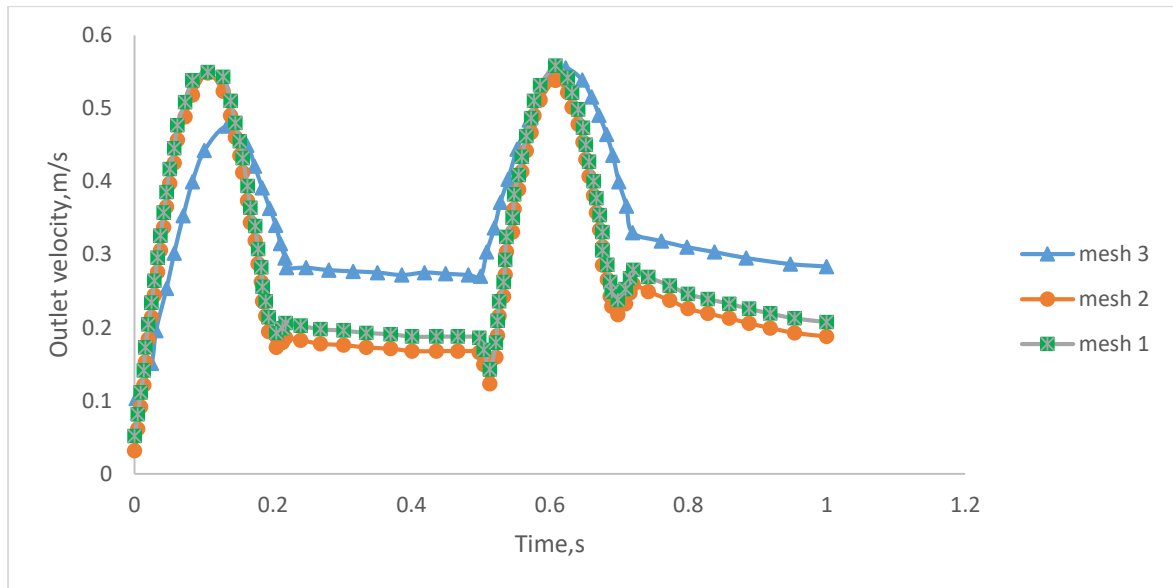


Fig: 4.8: Mesh sensitivity test result.

Table 4.6: Maximum velocity in three types of mesh

Mesh type	No. of elements	Maximum velocity
Coarse (mesh 3)	50,000	0.555271
Medium (mesh 2)	1,88,934	0.548369
Fine (mesh 1)	2,101,155	0.550011

CHAPTER 5

RESULTS AND DISCUSSION

5.1 General

Simulated results of the velocity, pressure, and wall shear stress for pulsating blood flow in the human aorta with three major branches are presented for the analysis in this chapter. These results regarding without magnetic effect are then compared with the MHD field.

5.2 Validation of the simulation

The numerical simulation must be checked using some analytical solution and numerical experiment with comparable unsteady laminar flows in the human aorta before the findings can be analyzed. The velocity profile and shear stress in the aortic arc are compared to Morris et al. (2005) numerical study, and there is a significant similarity in velocity and shear stress. The numerical result is also compared to Vasava and Paritosh (2012). By applying MHD Shit et al. (2018) and Teferi et al. (2021) found that the velocity is decreasing and wall shear stress is increasing. In arteries with Reynolds numbers less than 100, the flow passes through the branches without separation which is also observed in the calculation of Reynolds numbers.

5.2.1 Validation of velocity

Morris et al. (2005) designed a tapered ascending aorta in their study, but only one inlet and descending aorta as the outlet was used in this study. A comparison between their descending aorta velocity profile and shear stress results is performed in the present study, which is plotted in Fig. 5.2. The computational results are slightly varying from that of the experimental result in Morris et al. (2005) study due to some changes in geometrical design and also for the number of outlets. It is observable that the velocity profile increased to reach a peak and then they decrease as with the cross-sectional area.

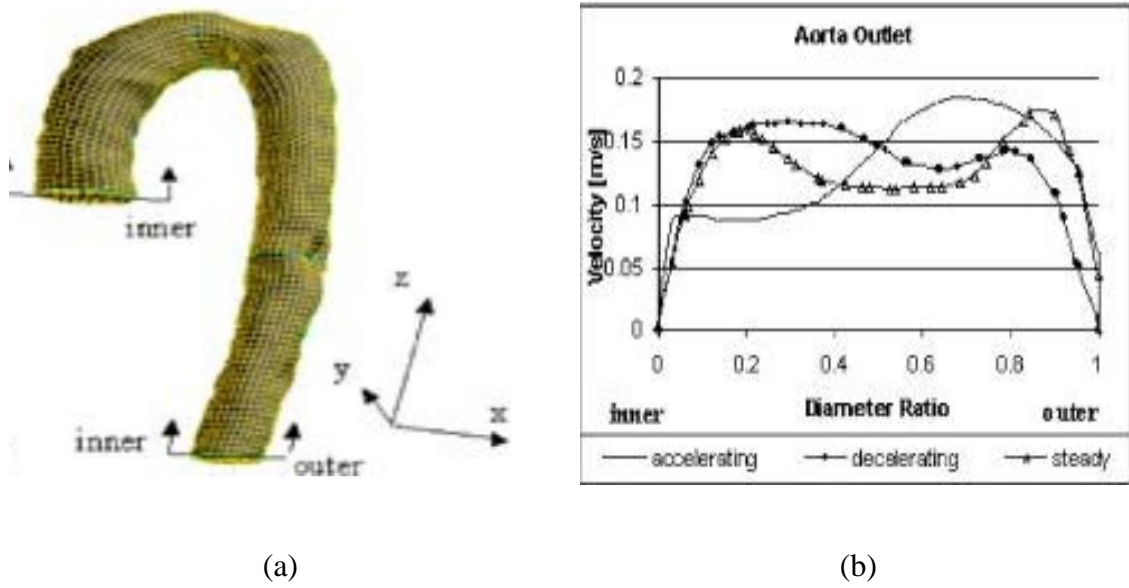


Fig. 5.1: (a) Geometry taken from Morries et al. (2005) (b) Descending aorta data from Morries et al. (2005).

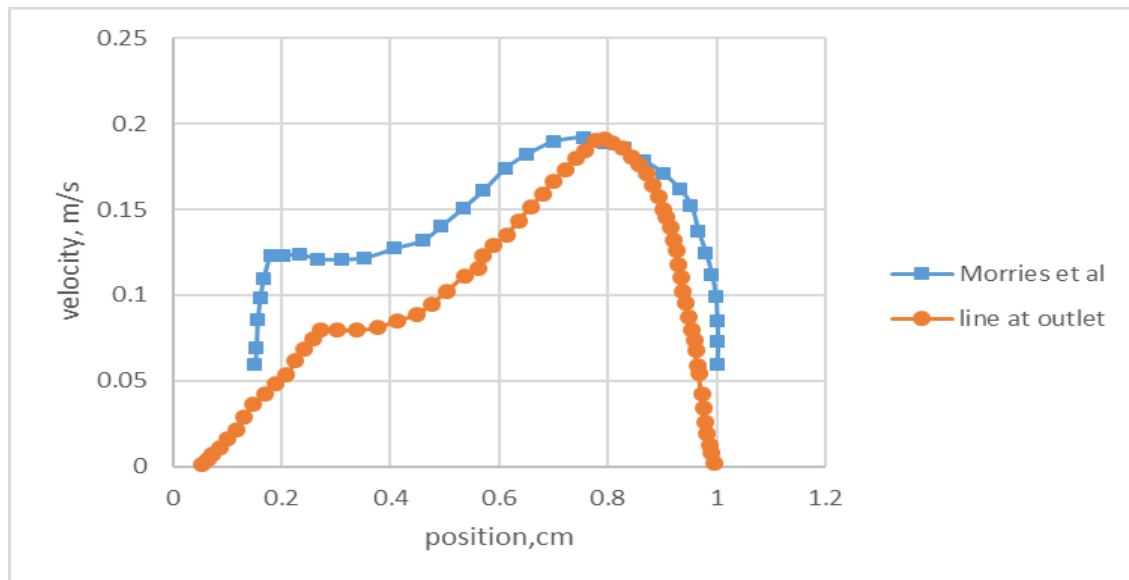


Fig. 5.2: Comparison of the present study in terms of velocity at the outlet with Morries et al. (2005).

5.2.2 Validation of Wall Shear Stress

In the case of wall shear stress, the numerical result is also compared with Morries et al. (2005). In their study, the maximum wall shear is found about 16 Pa while in the present study it is observed at 17 Pa.

5.2.3 Validation of VOF Model

In this simulation, blood is modeled as two-phase flow. According to Abidi et al. (2021) the experimental results showed that the pressure drop profile for two-phase flows is notably different from the one for single-phase flows in a very narrow microchannel, as was seen when earlier publications were examined. Lyras and Lee (2022) designed a cylinder shaped with a stenosis Non-Newtonian blood model and compared both single phase and two phase model. Lyras and Lee (2022) state that ‘Neither pressure drop nor mean velocity are not strongly changed in the multiphase modelling, but particle buildup significantly changes which is only revealed by the multiphase approach.’ Fig. 5.3 shows that there is slightly drop in the outlet pressure with respect to flow time.

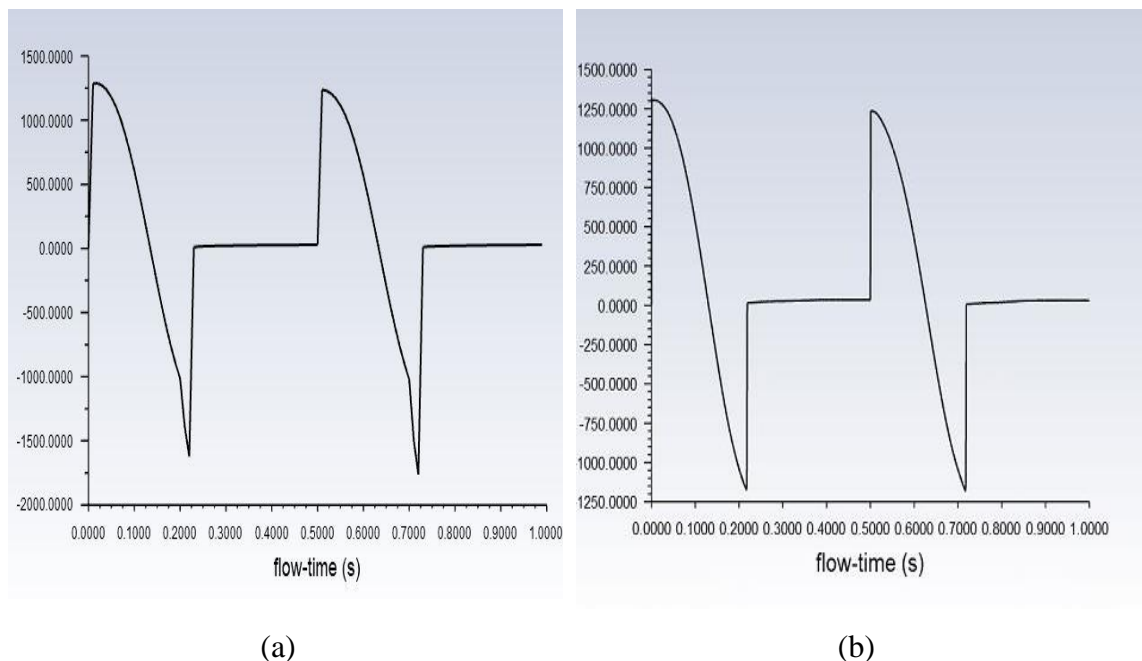


Fig. 5.3: Outlet pressure profile with time (a) single phase (without VOF model) (b) two-phase (VOF model).

5.2.4 Validation of MHD

Altintas and Ozkol (2015) investigated MHD field on a 300 mm long and 10 mm diameter pipe to observe the impact of sodium potassium liquid behavior. According to their study, as MHD field is applied the velocity profile is observed to decrease its value.

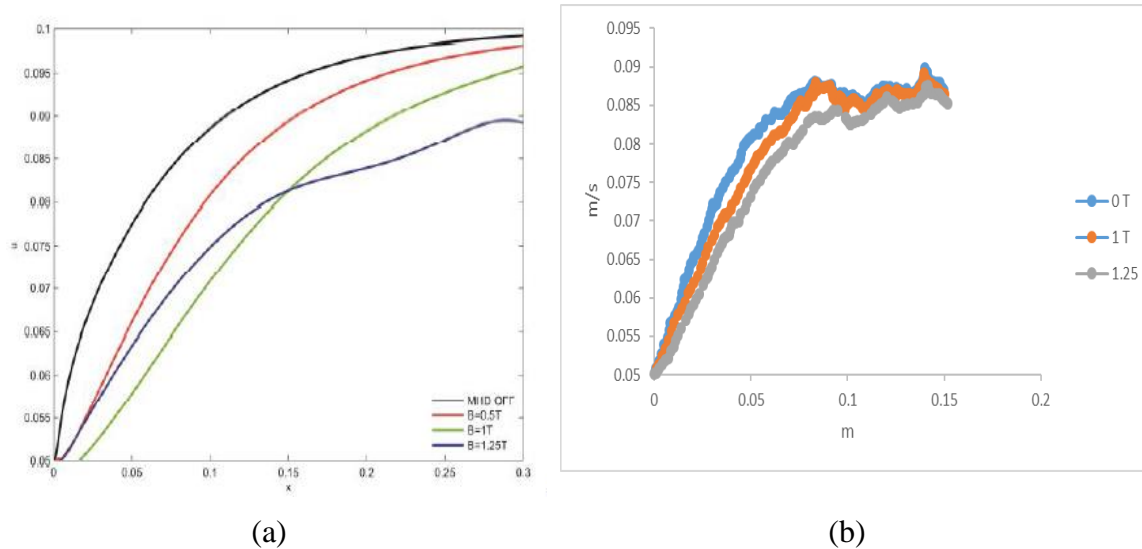


Fig. 5.4: (a) Taken from Altintas and Ozkol (2015) (b) Velocity vs position

5.3 Computational Results

In this section, the computational results will be discussed at the designed pulsating velocity for 1 sec. A comparison between the non-magnetic field results with the magnetic field computational results and the percentage of variation will be discussed. One inlet, four outlets, and two planes have been chosen to demonstrate the difference for MHD. Fig. 5.4 shows the selected planes and lines along with the inlet and outlets sections. Changes in terms of velocity, pressure, and wall shear stress are discussed.

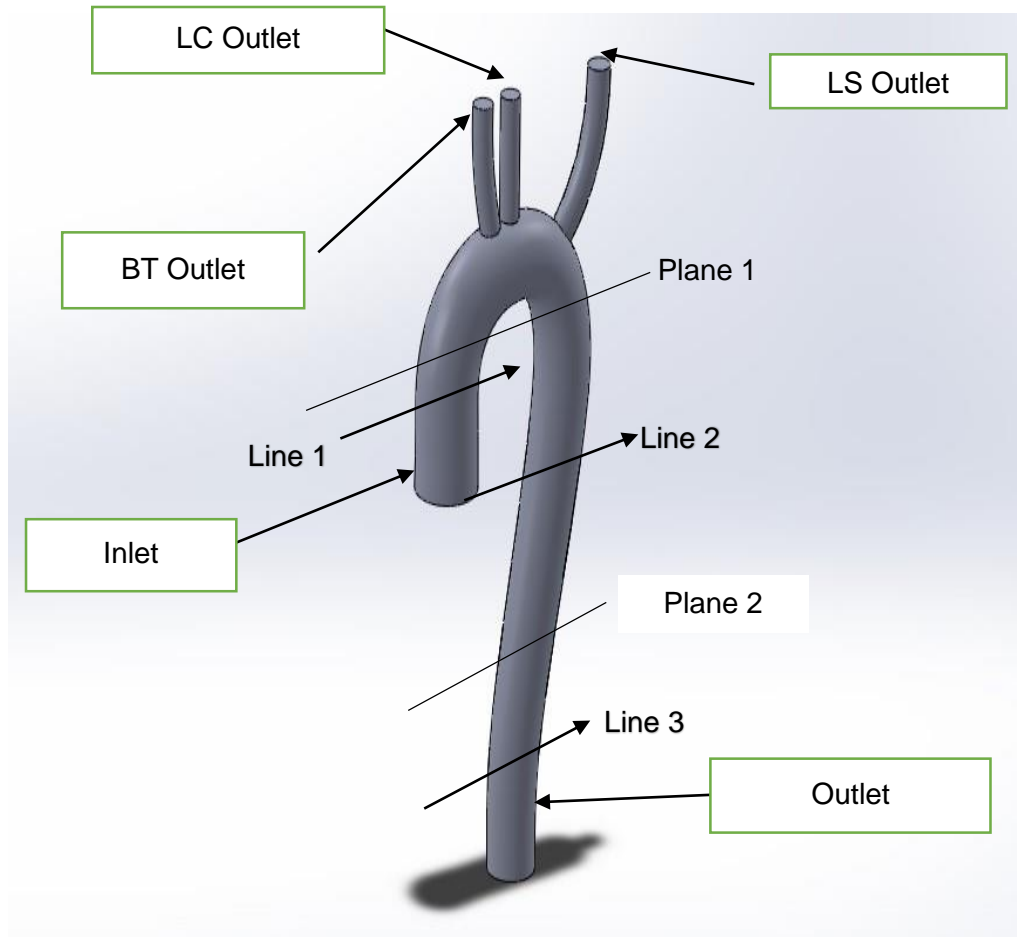


Fig. 5.5: Selected planes and lines with inlet and outlets.

5.3.1 Comparison of Velocity

From Fig. 5.5 to Fig. 5.15 shows the numerical results for velocity contour which are represented for ascending aorta inlet, BT outlet, LC outlet, LS outlet, descending Outlet, plane 1, plane 2, xy cross-sectional plane, line 1, line 2, and line 3.

5.3.1.1 Velocity at Inlet

As inlet velocity is designed as an unsteady pulsating waveform, the ascending aorta shows no significant difference there. For 1 Tesla magnetic field which is applied to generate this present study. The inlet flow is found fully laminar.

Inlet velocity without MHD

Inlet velocity with MHD

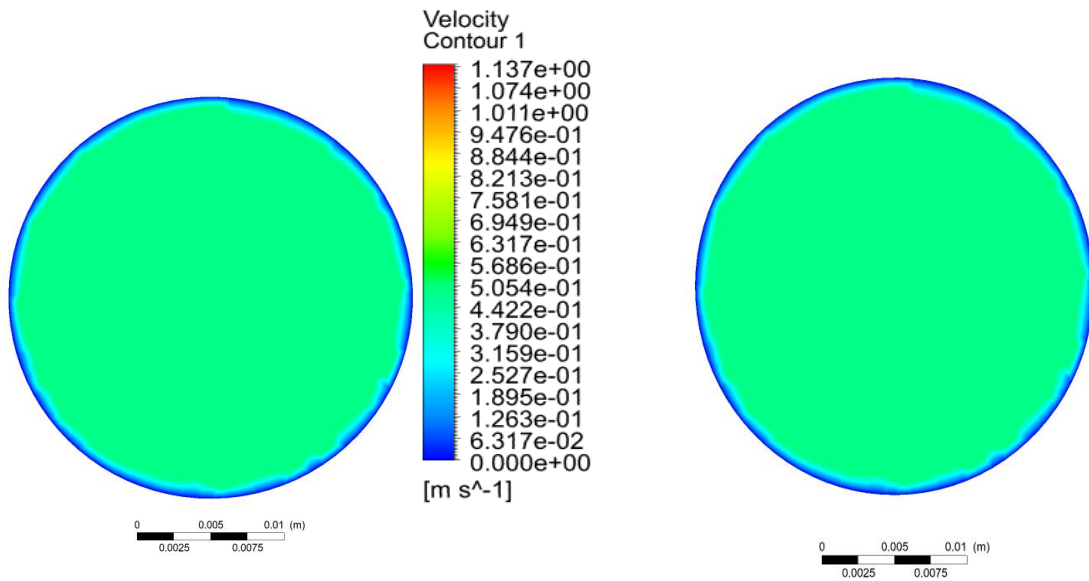
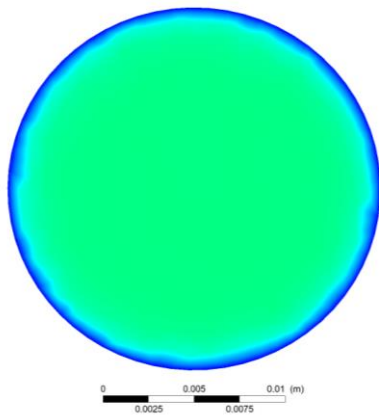


Fig 5.6: Inlet velocity contour.

5.3.1.2 Comparison of Velocity at Outlets

From Figure 5.6 to 5.15 illustrates the changes in contour velocity for applying MHD to blood flow. There is no slip condition so the outer wall velocity is zero and it increases at the center. As 1 Tesla magnetic field is applied, the velocity profile is decreasing. The velocity profile is fully developed at the center so the xy cross-section which is at the middle plane is selected for this transient analysis. Table 5.1 shows the difference in velocity due to the magnetic effect. As MHD is applied for this selected aorta section, blood velocity is decreasing. Fig. 5.13 also represents a simple line at the descending aorta section velocity with and without MHD. It is clear that applying 1 Tesla magnetic field the flow is diminishing. Because the Lorentz force tends to counter blood flow as a magnetic field is introduced to the body, the velocity drops. Because red blood cells in blood contain ions, the Lorentz force can counteract the motion of blood flow. Both Kumari et al. (2019) and Sharma et al. (2019), who took the Navier slip into consideration, came to similar conclusions.

Outlet velocity without MHD



Outlet velocity with MHD

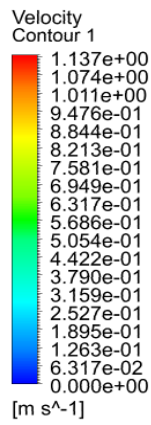
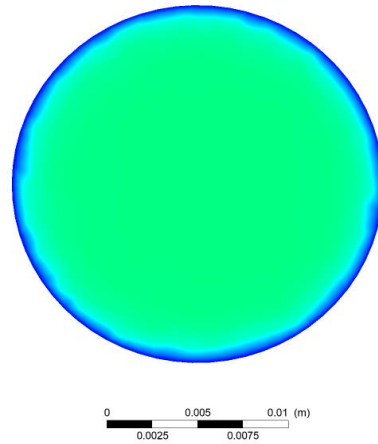
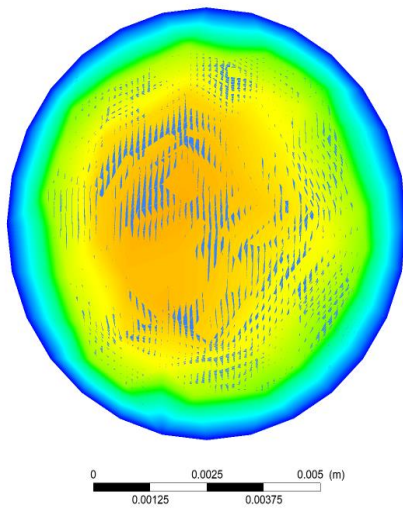


Fig. 5.7: Outlet velocity contour.

BT Outlet velocity without MHD



BT Outlet velocity with MHD

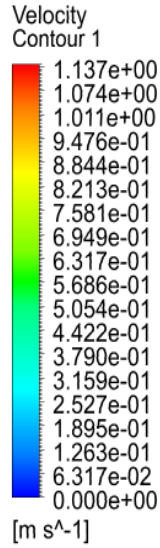
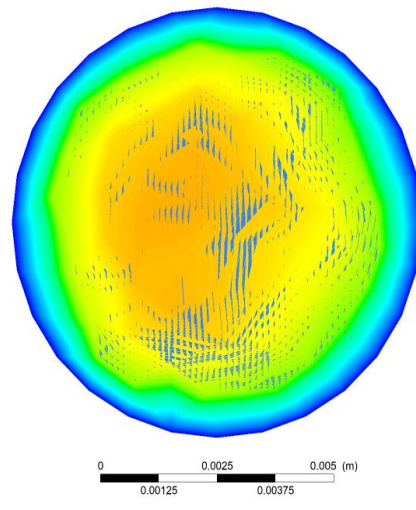
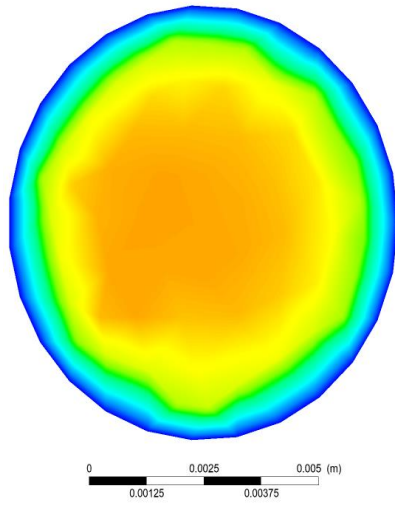


Fig. 5.8: BT Outlet velocity contour.

LC Outlet velocity without MHD



LC Outlet velocity with MHD

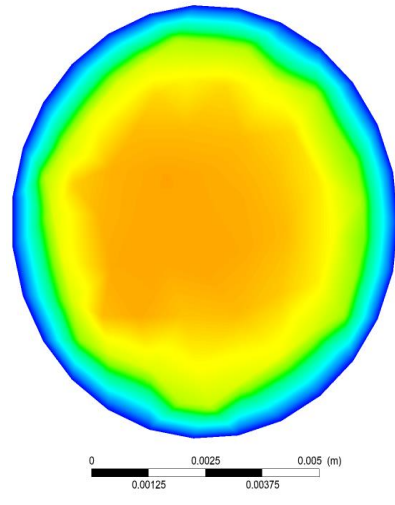
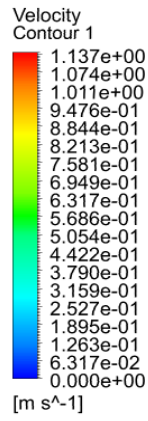
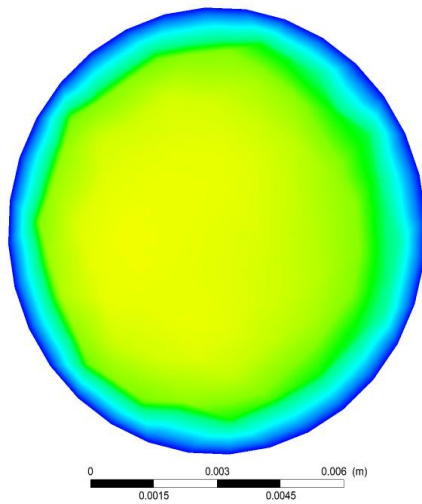


Fig. 5.9: LC Outlet velocity contour.

LS Outlet velocity without MHD



LS Outlet velocity with MHD

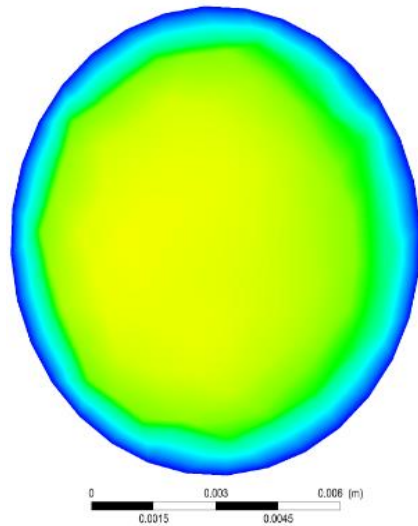
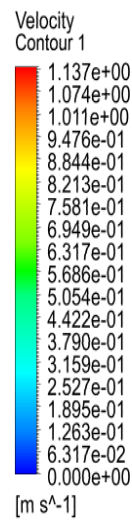
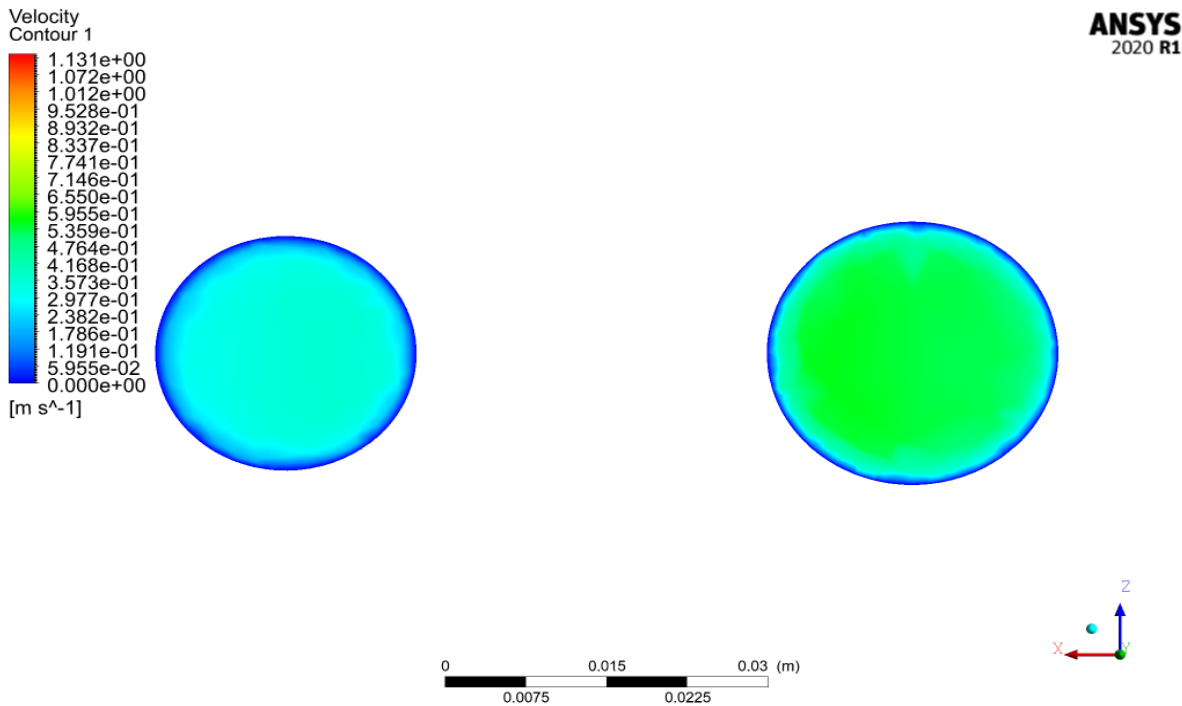


Fig. 5.10: LS Outlet velocity contour.

Plane 1 velocity without MHD



Plane 1 velocity with MHD

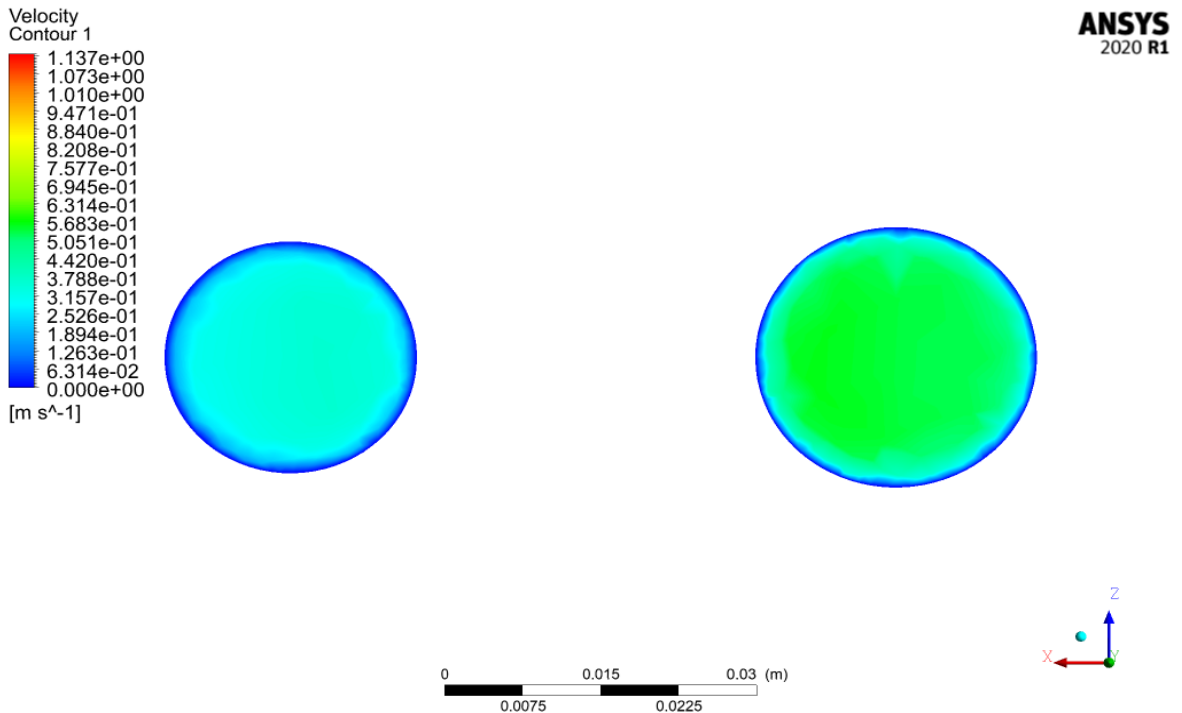


Fig. 5.11: Plane 1 velocity contour.

Plane 2 velocity without MHD

Plane 2 velocity with MHD

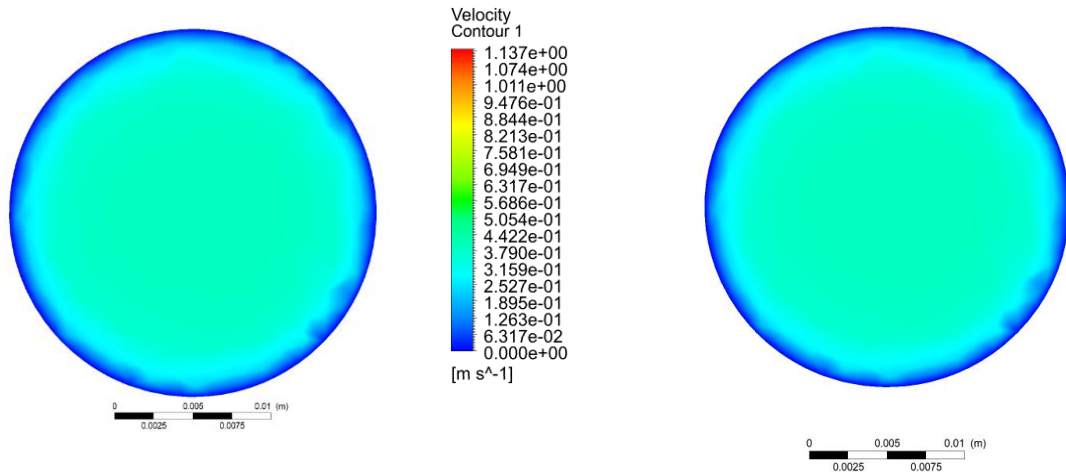


Fig. 5.12: Plane 2 velocity contour.

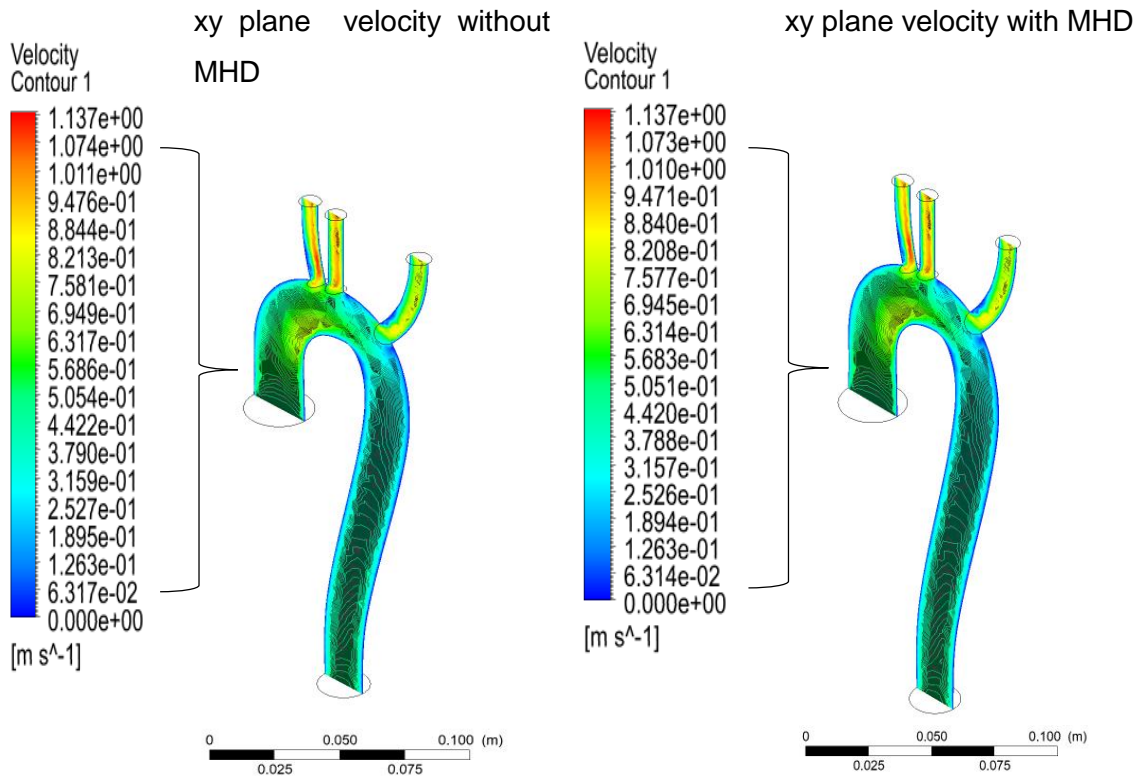


Fig. 5.13: xy cross-sectional velocity contour.

Table 5.1: Numerical comparison of velocity due to MHD (1 Tesla)

Without MHD (m/s)	Average velocity	With MHD (m/s)	Average velocity	Difference	%
1.074	0.5739	1.073	0.5737	0.0002	0.035%
1.1011		1.1010			
0.9476		0.9471			
0.8844		0.8840			
0.8213		0.8208			
0.7581		0.7577			
0.6949		0.6945			
0.6317		0.6314			
0.5686		0.5683			
0.5054		0.5051			
0.4422		0.4420			
0.3790		0.3788			
0.3159		0.3157			
0.2527		0.2526			
0.1895		0.1894			
0.1263		0.1263			
0.06317	0.06314				

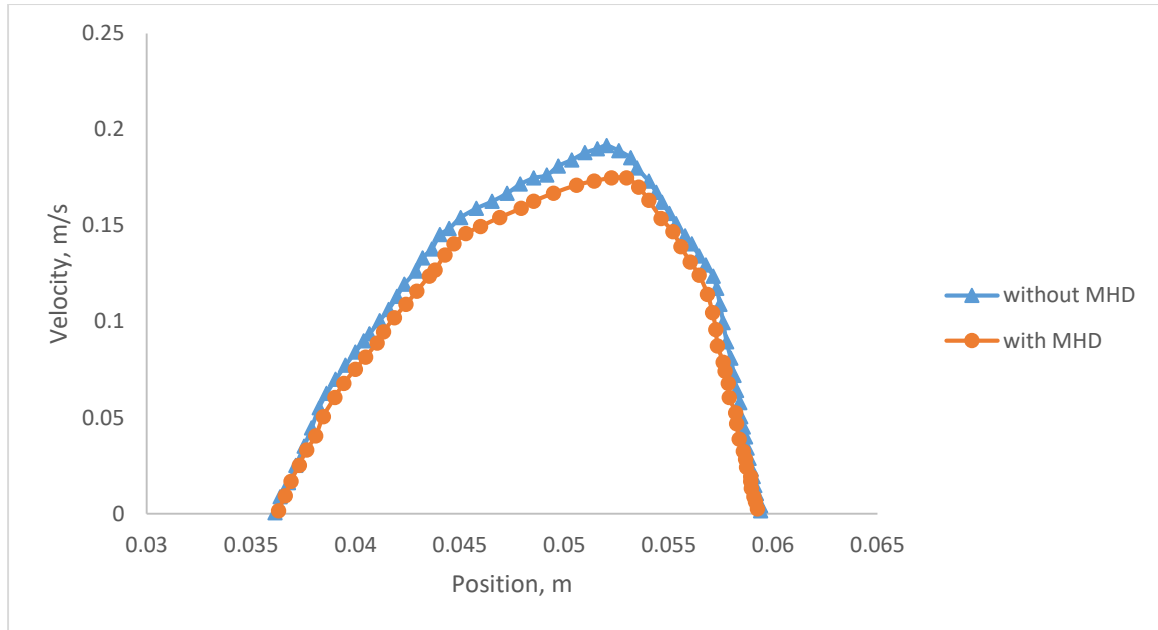


Fig. 5.14: Comparison of velocity profile in line at descending aorta.

5.3.1.3 Comparison of velocity with time

Human blood is considered to be pulsating by using a UDF. For given two pulses in 1 second as inlet, the following Fig: 5.14 shows the outlet of the aorta section. By comparing it is observed that the maximum velocity point is not vary. However, the lowest velocity points are decreasing by the effect of MHD field which is shown in the Fig: 5.15.

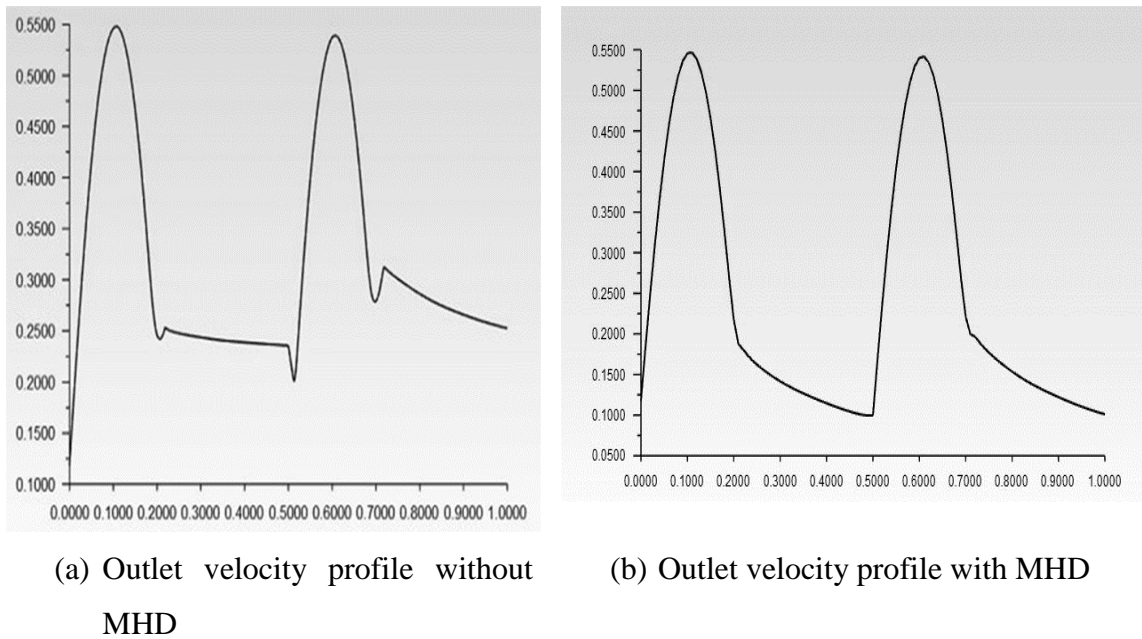


Fig. 5.15: Outlet velocity profile with time.

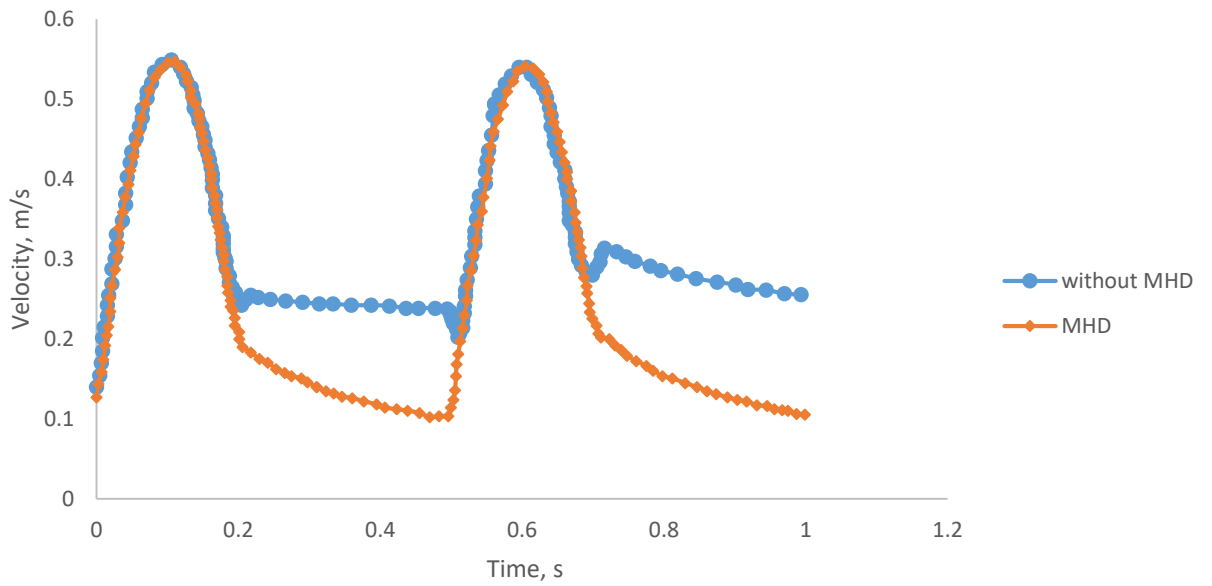


Fig. 5.16: Comparison of outlet velocity profile with time.

5.3.1.4 Comparison of velocity in three different lines in their respective planes

Velocity comparison for 1 Tesla ($y = 30\text{mm}$)

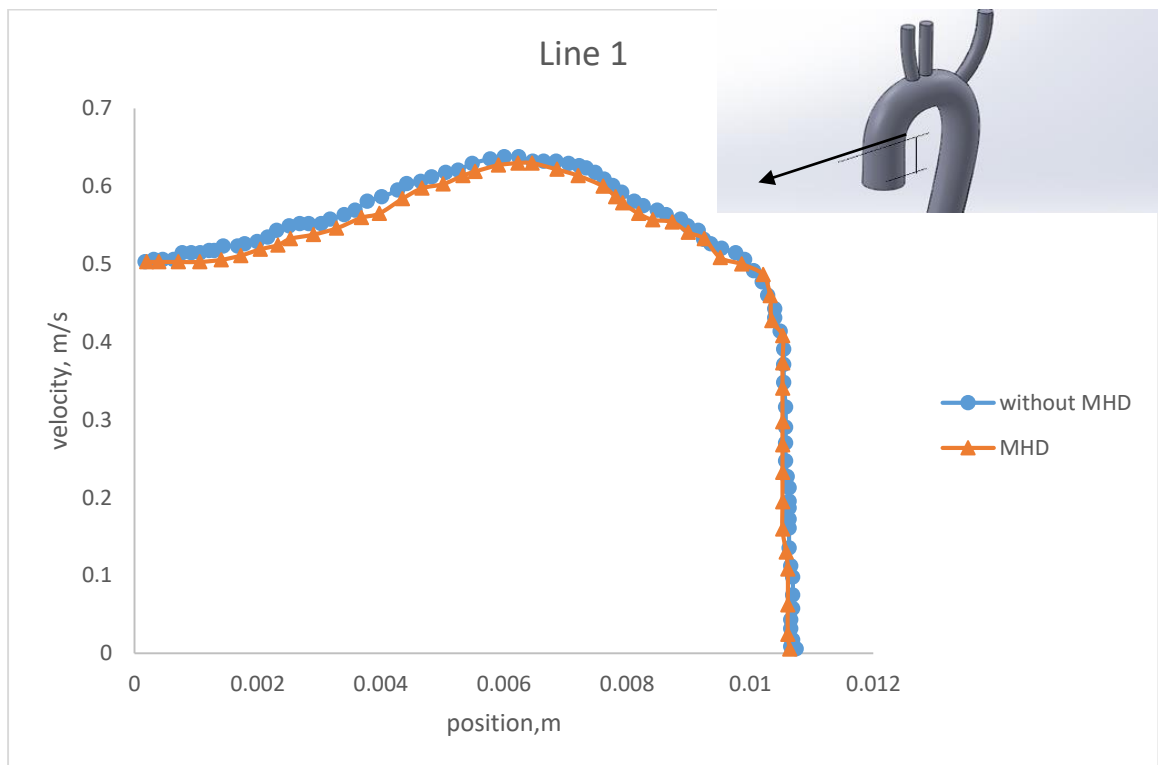


Fig. 5.17: Comparison of velocity at $y = 30\text{mm}$ (Line 1).

Velocity comparison for 1 Tesla ($y = -60\text{mm}$)

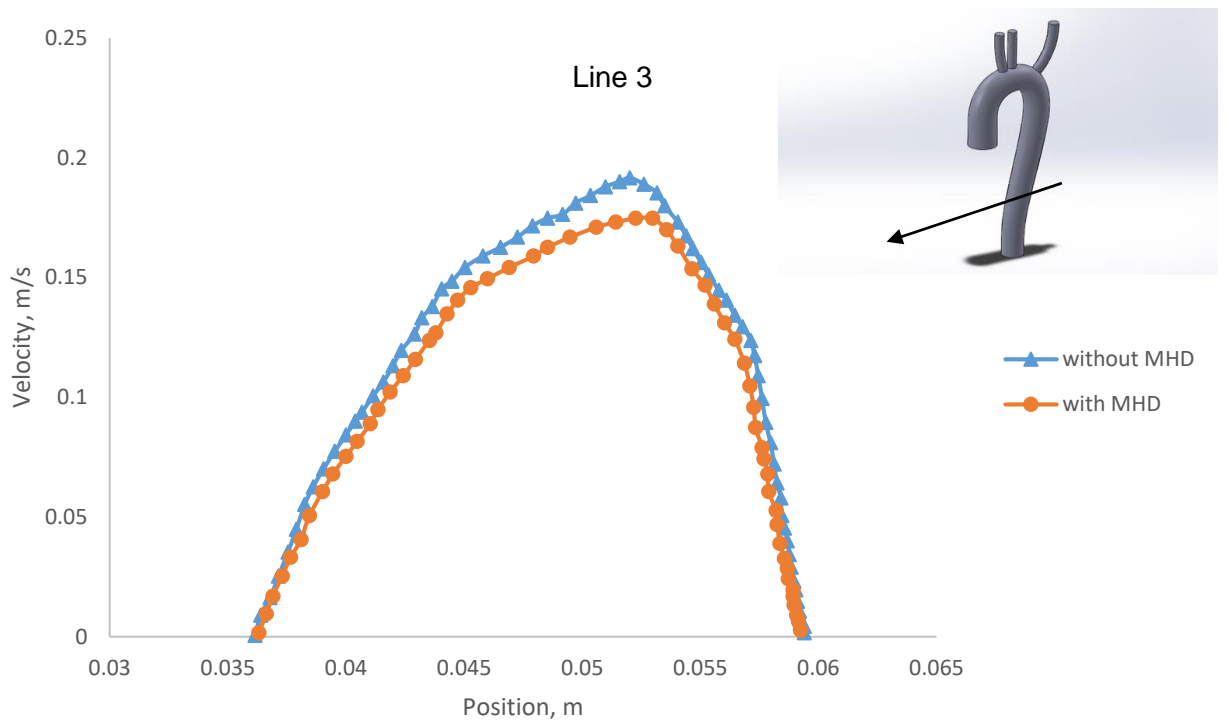


Fig. 5.18: Comparison of velocity at $y = -60\text{mm}$ (Line 3).

Velocity comparison for 1 Tesla (descending aorta)

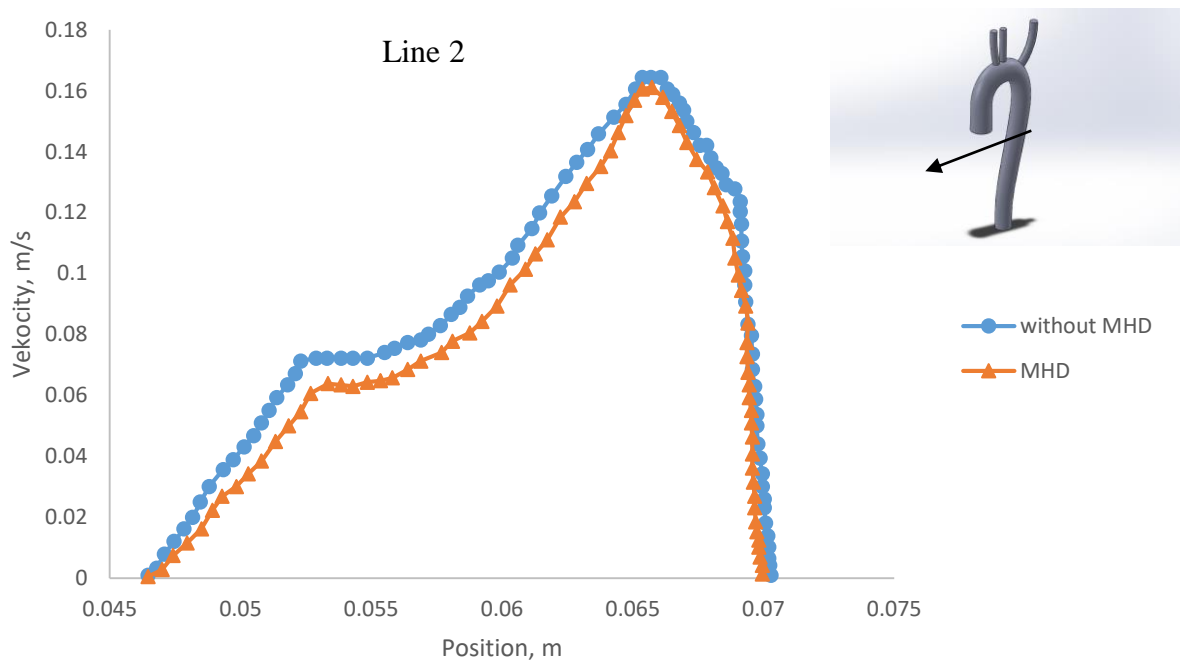


Fig. 5.19: Comparison of velocity at line 2.

5.3.2 Comparison of Pressure

Figure 5.17 to 5.20 illustrate the variation of the pressure distribution for incorporating the pulsating velocity with respect to with and without MHD at unsteady conditions. Here, static pressure is observed with zero gauge pressure. In ascending aorta section which is consider as inlet, there is no changes for applying MHD. However, variation in pressure is found as the length of the aorta is increasing.

Static pressure without MHD

Static pressure with MHD

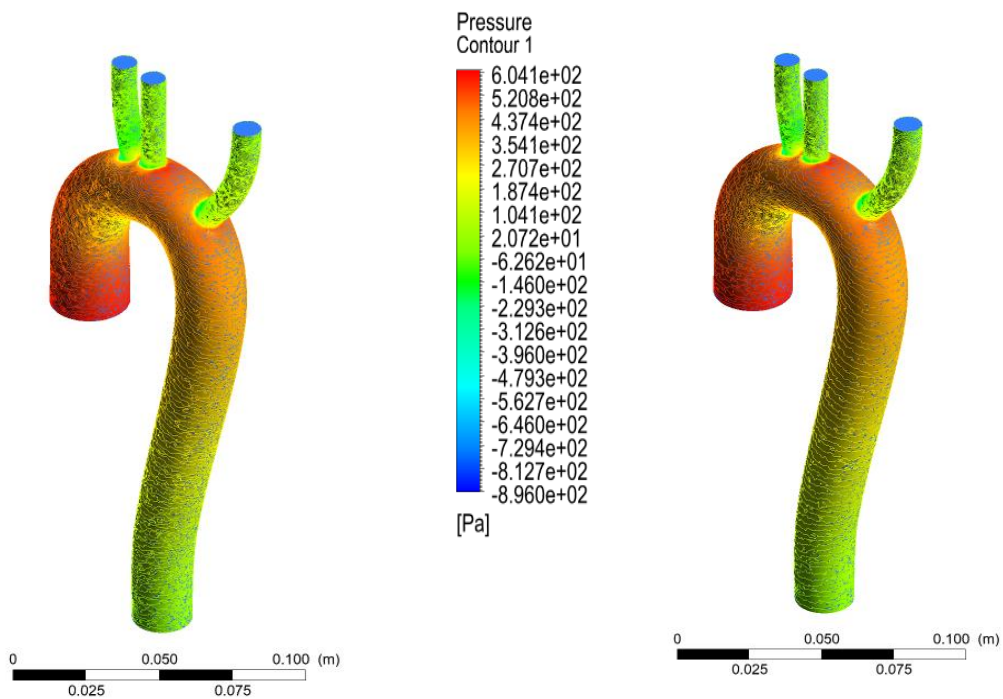


Fig. 5.20: wall static pressure contour.

Inlet pressure without MHD

Inlet pressure with MHD

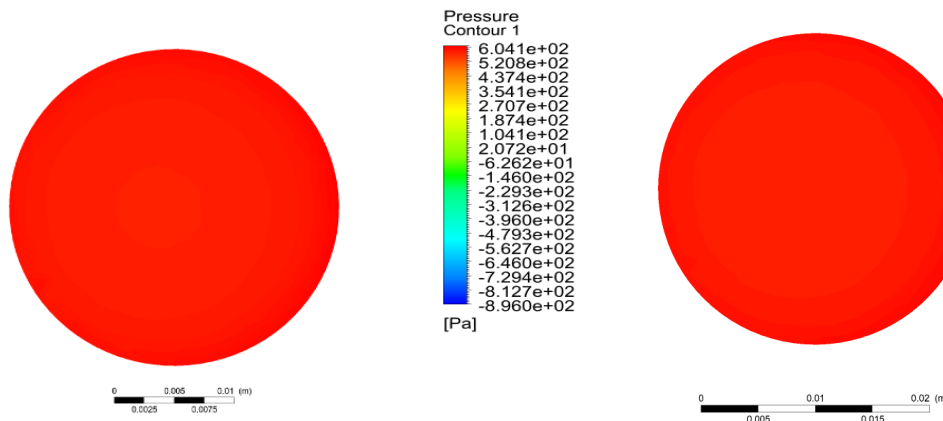
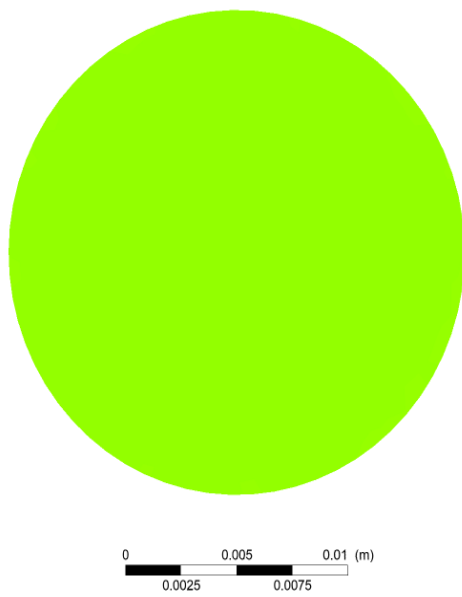


Fig. 5.21: Inlet pressure contour.

Outlet pressure without MHD



Outlet pressure with MHD

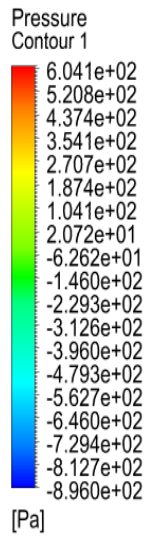
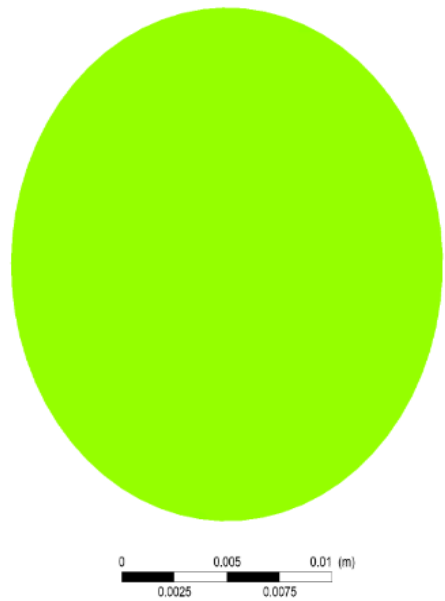
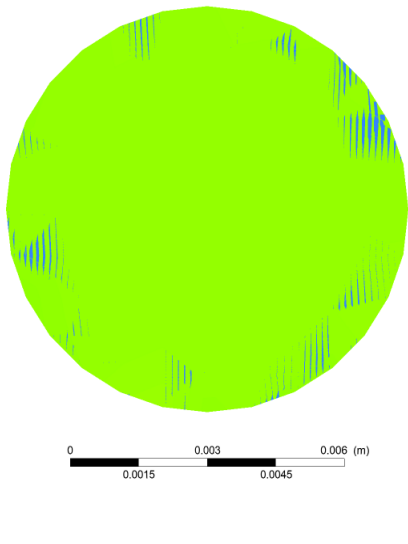


Fig. 5.22: Outlet pressure contour

BT Outlet pressure without MHD



BT Outlet pressure with MHD

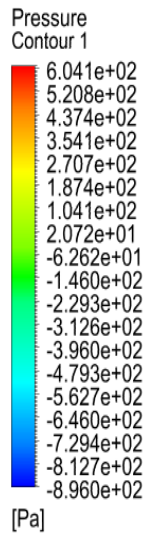
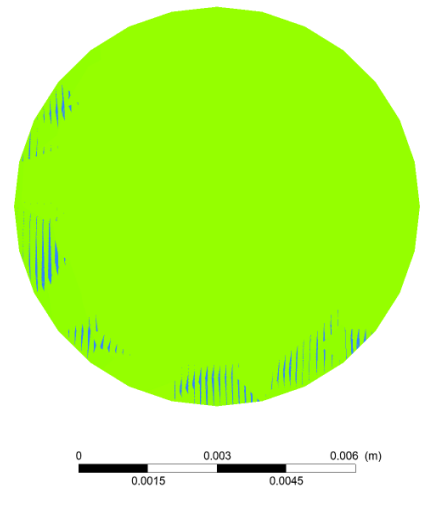
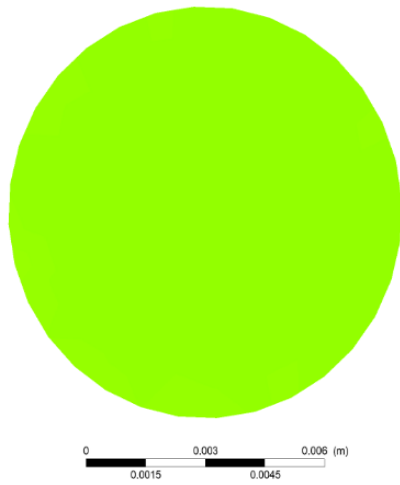


Fig. 5.23: BT Outlet pressure contour.

LS Outlet pressure without MHD



LS Outlet pressure with MHD

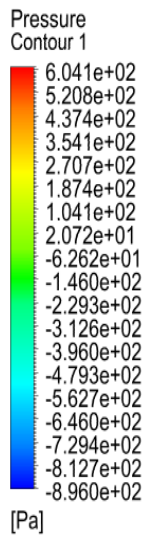
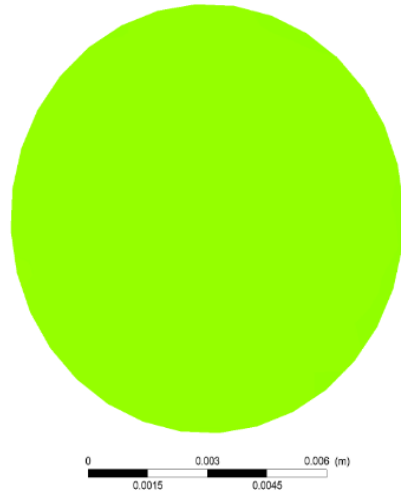
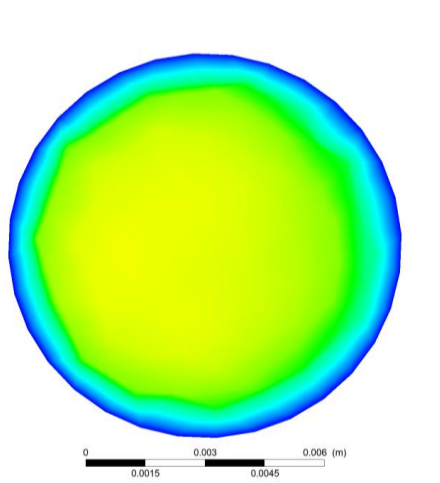


Fig. 5.24: LS Outlet pressure contour.

LC Outlet pressure without MHD



LC Outlet pressure with MHD

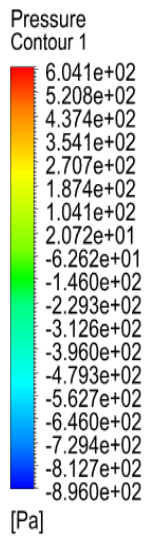
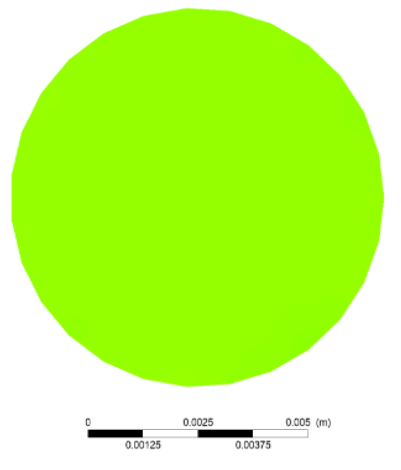
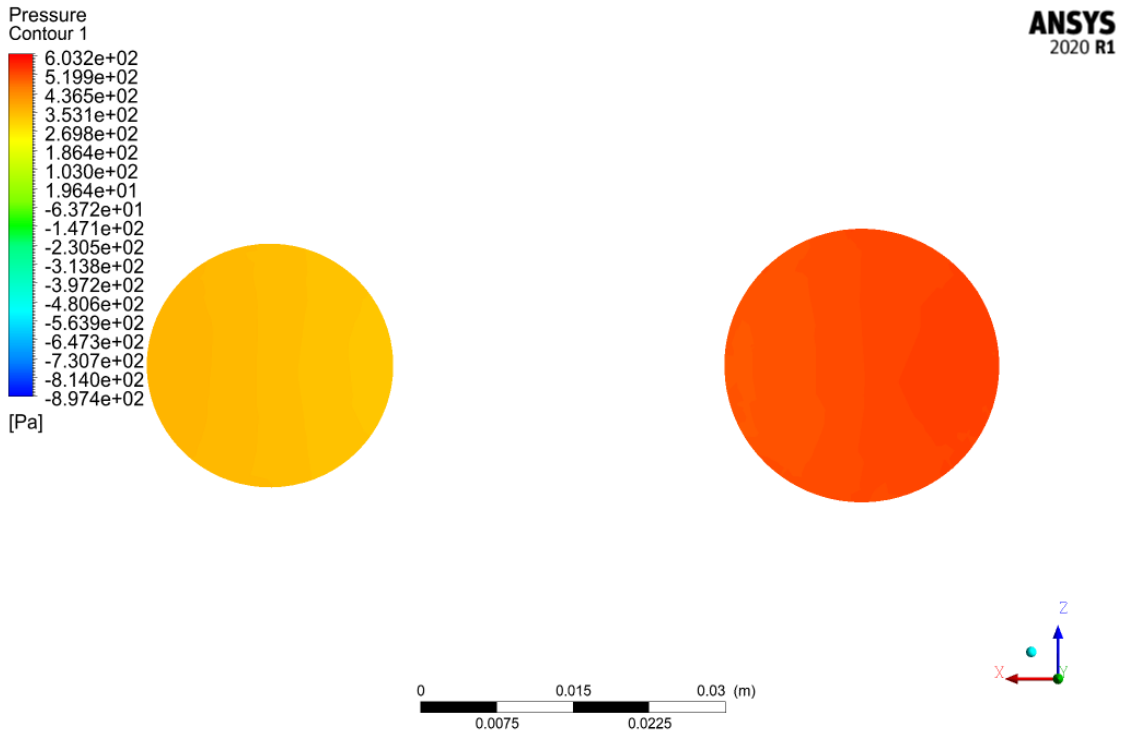


Fig 5.25: LC Outlet pressure contour.

Plane 1 pressure without MHD



Plane 1 pressure with MHD



Figure 5.26: Plane 1 pressure contour.

Plane 2 pressure without MHD

Plane 2 pressure with MHD

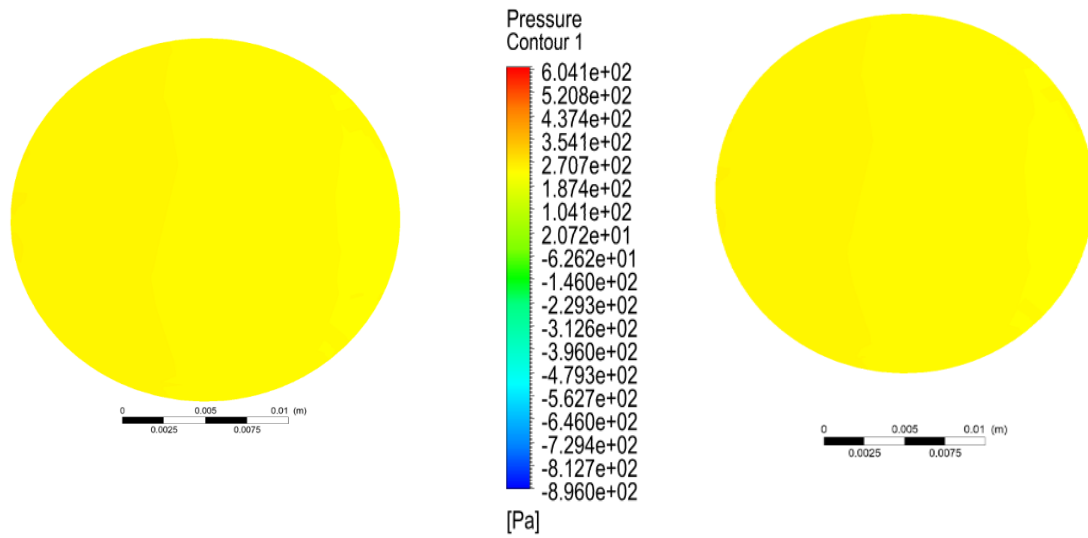


Fig. 5.27: Plane 2 pressure contour.

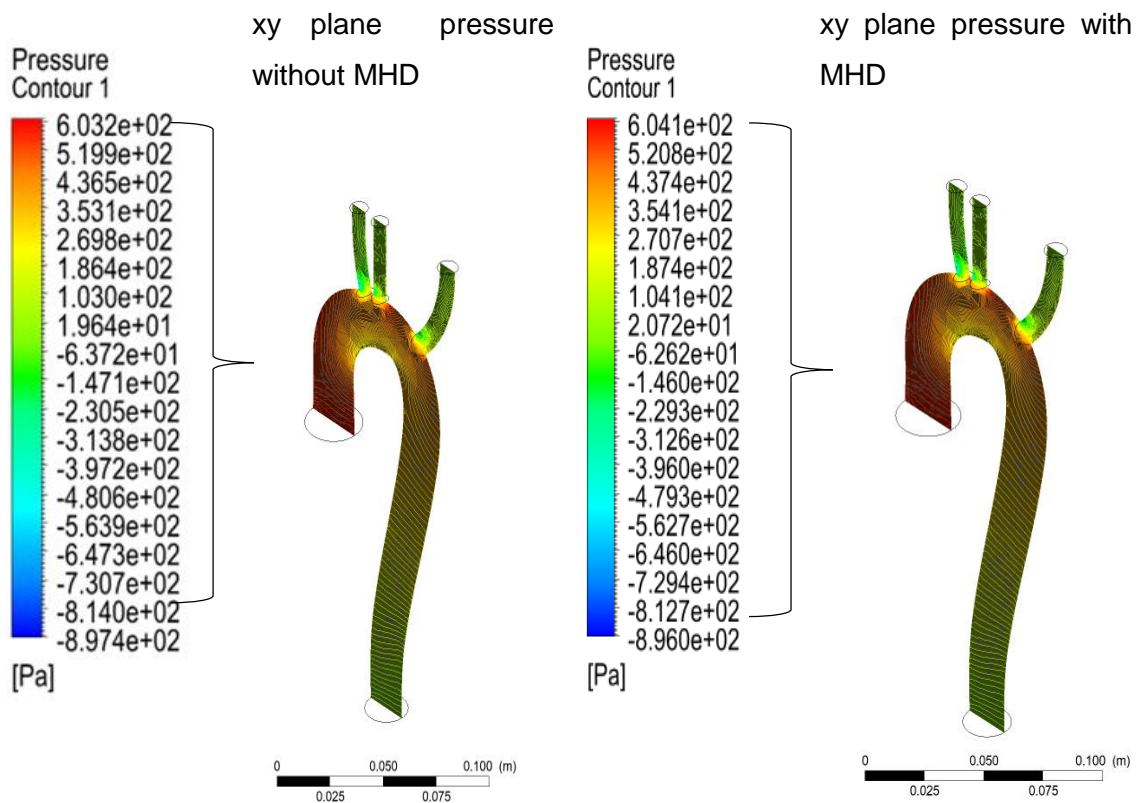


Fig. 5.28: xy cross sectional plane pressure contour.

If we set the diastolic blood pressure as inlet pressure which is 80 mmHg, then the value of height pressure generate is 90mmhg. Fig. 5.26 shows the pressure distribution over time.

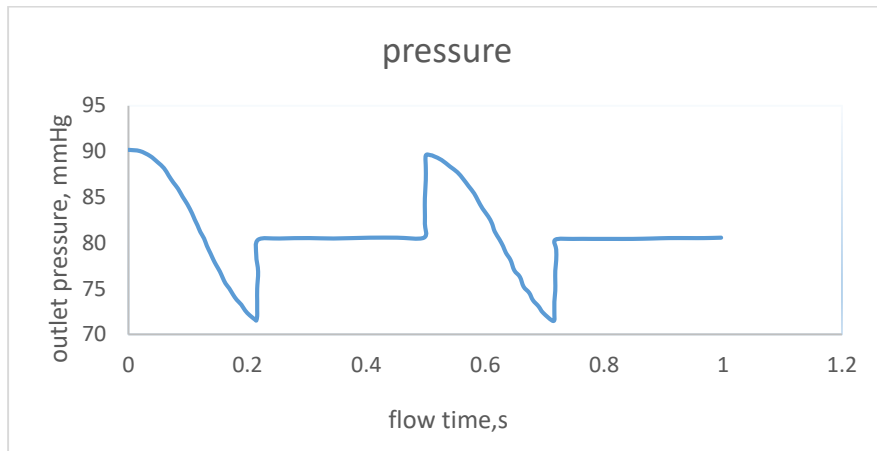


Fig. 5.29: pressure distribution for diastolic cycle.

5.3.2.1 Comparison of pressure with time

By applying 1 Tesla magnetic field, the static pressure increases about 9%. Fig 5.27 shows the pressure profile with respect to flow time.

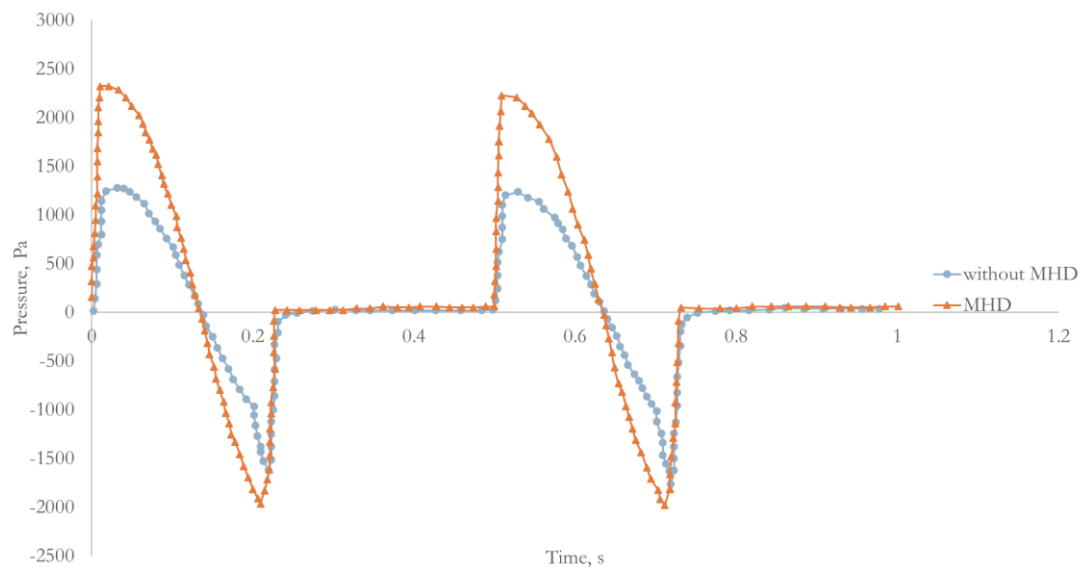


Fig. 5.30: Comparing pressure distribution with and without MHD.

5.3.3 Comparison of Wall Shear Stress

In case of shear stress, the value of wall shear stress increases as MHD is applied. The height value of wall share stress is 17.9 Pa while applying MHD field the value shows a rise about 18.56 Pa. Figure 5.28 and 5.29 illustrate the wall shear stress contour without and with MHD respectively. Results are indicating that after applying magnetic field, the wall shear stress is increasing.

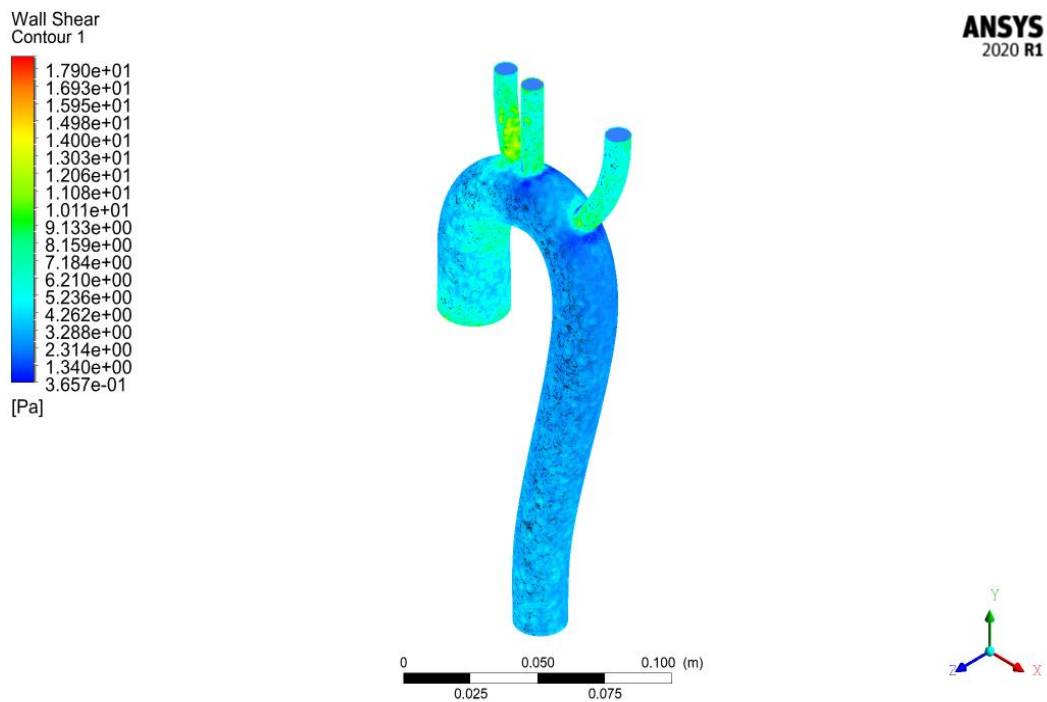


Fig. 5.31: Wall shear stress without MHD.

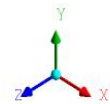
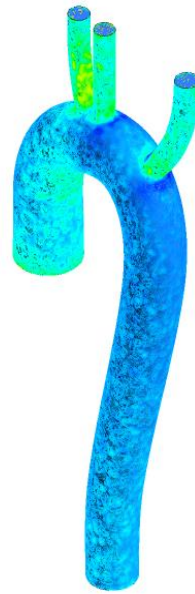
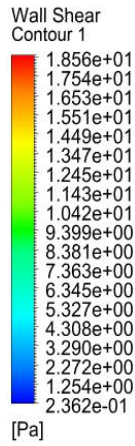
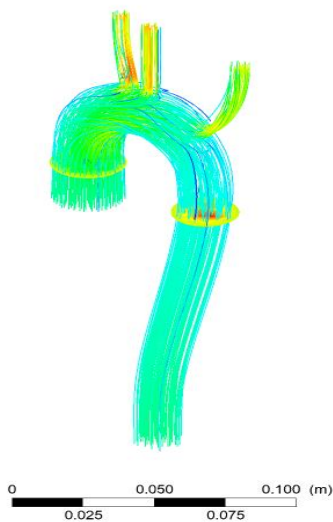


Fig.5.32: Wall shear stress with MHD .

5.3.4 Variation of Velocity Streamlines

The velocity streamline tells us that there is no backflow happening in this simulation. As velocity is a vector quantity it has both value and magnitude.

Velocity stream line without
MHD



Velocity stream line with MHD

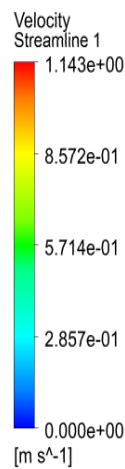
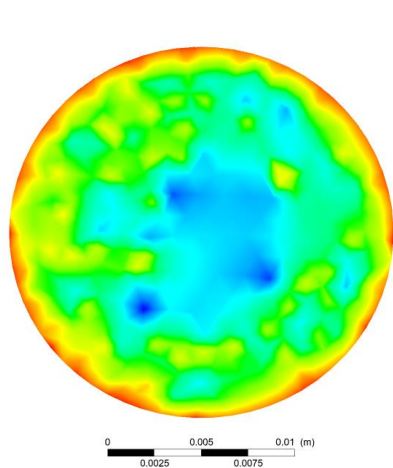


Fig. 5.33: velocity streamline.

5.3.5 Comparison of Mass Flow Rate

From fig. 5.31 to 5.38 mass flow through different arteries section have been illustrate. It is seen that by applying MHD the mass flow is increasing. (-) ve sign indicates the outlet mass and (+) ve sign indicates the inlet mass through the aorta.

Outlet Mass flow without MHD



Outlet Mass flow with MHD

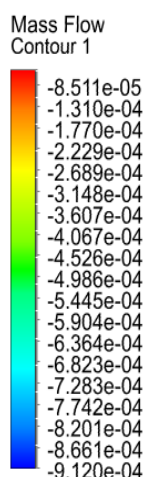
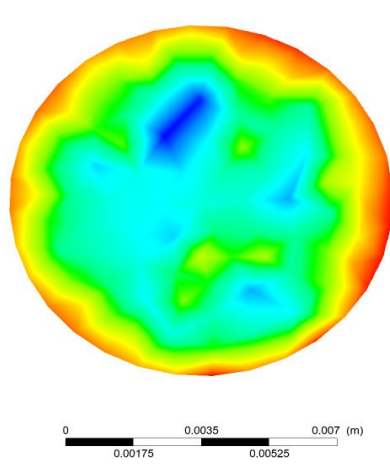
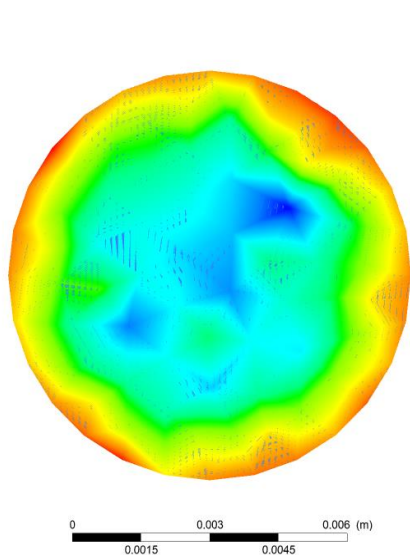


Fig. 5.34: Outlet mass flow.

BT Outlet Mass flow without MHD



BT Outlet Mass flow with MHD

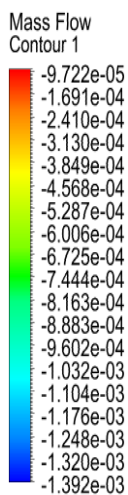
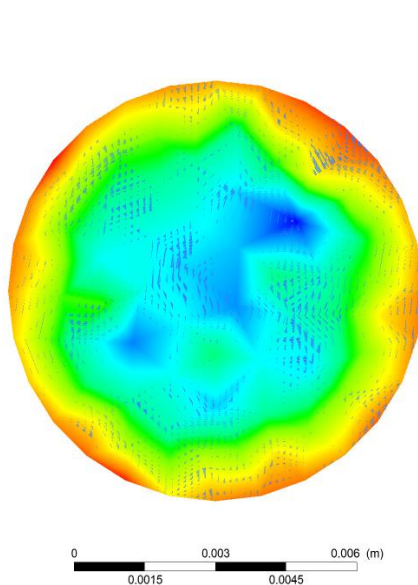


Figure 5.35: BT Outlet mass flow.

LS Outlet Mass flow without
MHD

LS Outlet Mass flow with MHD

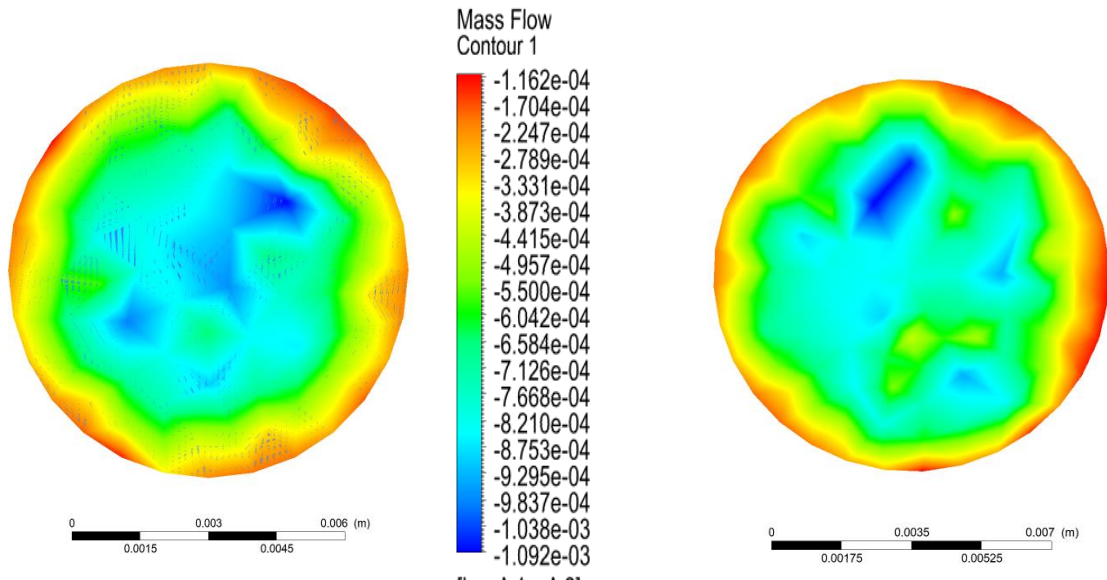


Fig. 5.36: LS Outlet mass flow.

LC Outlet Mass flow without
MHD

LC Outlet Mass flow with MHD

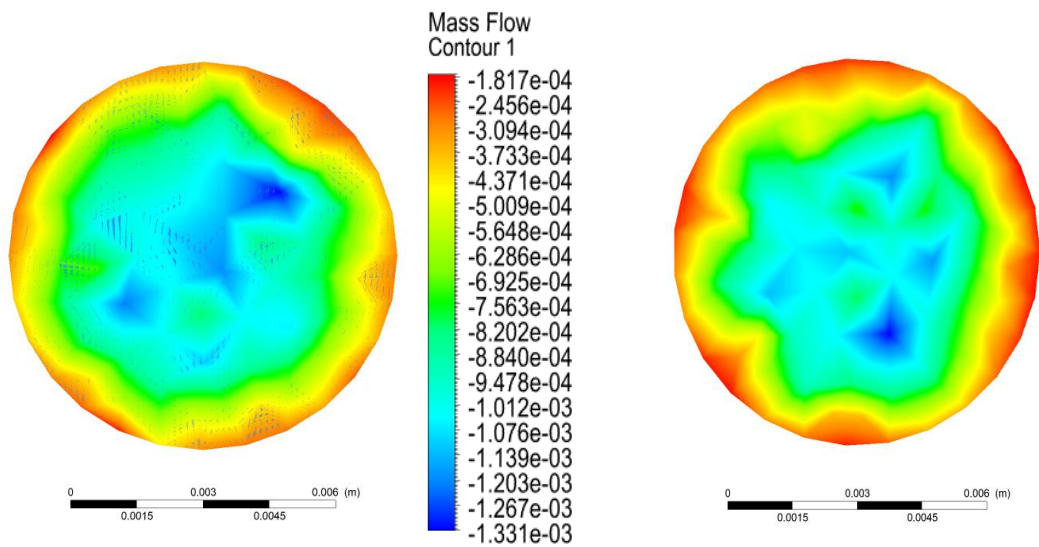
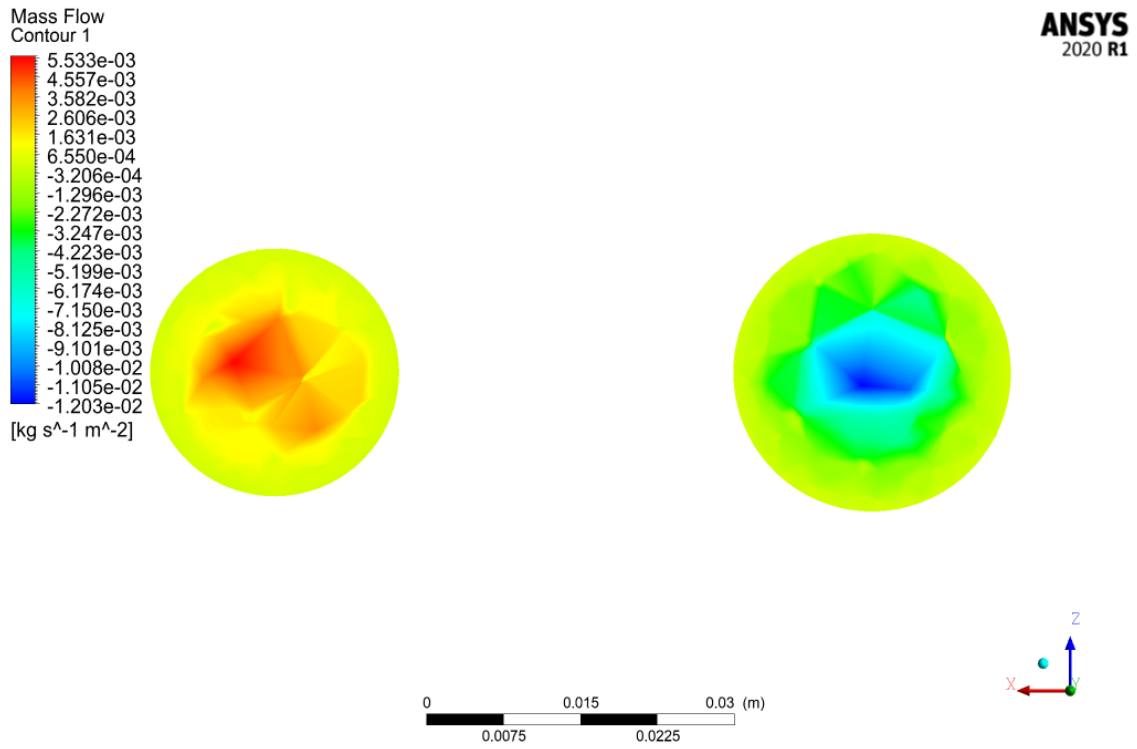


Fig. 5.37: LC Outlet mass flow.

Plane 1 Mass flow without MHD



Plane 1 pressure with MHD

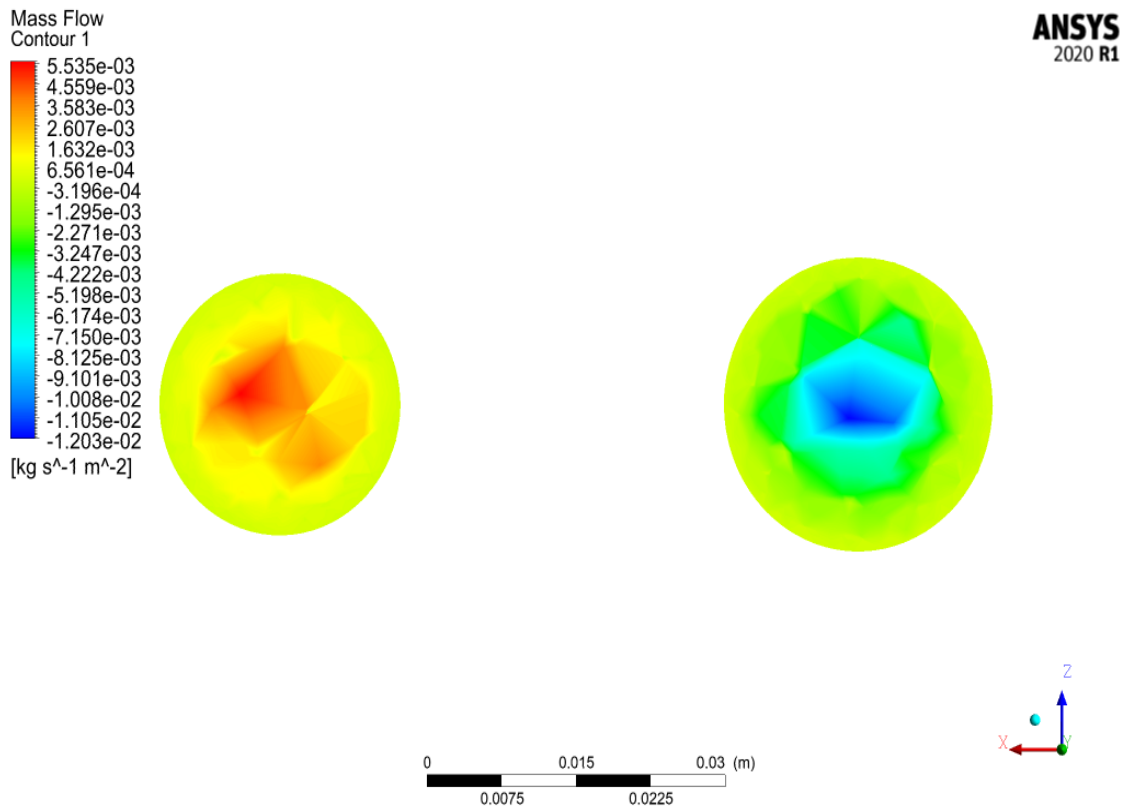


Fig. 5.38: Plane 1 mass flow.

Plane 2 Mass flow without MHD

Plane 2 Mass flow with MHD

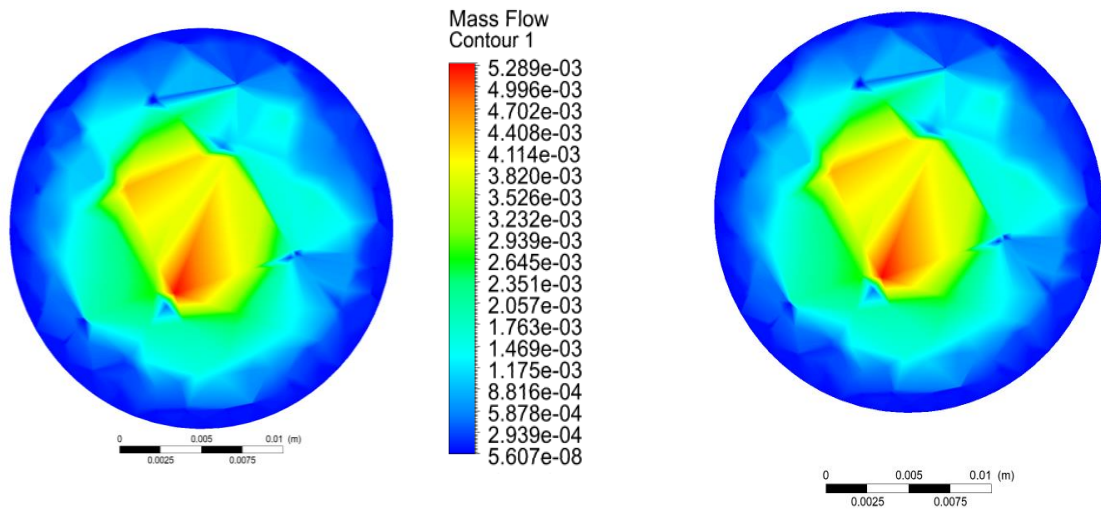


Fig. 5.39: Plane 2 mass flow.

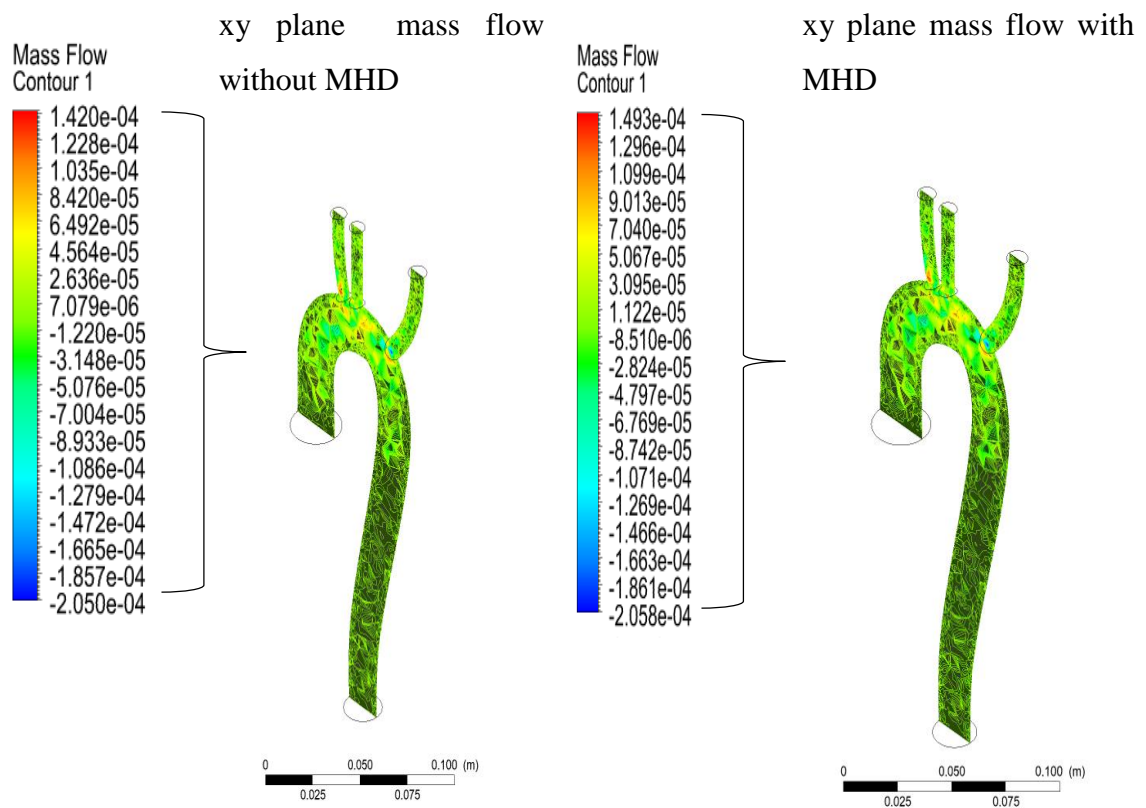


Fig. 5.40: xy cross-sectional plane mass flow

CHAPTER 6

CONCLUSIONS AND RECOMMENDATIONS

6.1 Concluding Remarks

This present study demonstrates a real three-dimensional geometry of the human aorta section with time variation for a design pulsating velocity. VOF model is designed for two-phase flow and incorporated both on the magnetic and non-magnetic effect to observe the changes in velocity, pressure and mass flow rate. From the analysis, the following conclusions are drawn:

- a) For pulsating flow Reynolds number is observed and the flow is fully laminar.
- b) On the basis of this simulation, it can be concluded that an external magnetic field (1 tesla) has an impact on arteries. By applying the MHD field, the value of average velocity is decreasing about 0.035% in the artery center point. Because the Lorentz force tends to counter blood flow as a magnetic field is introduced to the body, the velocity drops. Because red blood cells in the blood contain ions, the Lorentz force can counteract the motion of blood flow.
- c) In terms of pressure, mass flow, and wall shear stress, an increase about 9% is observed by applying MHD.
- d) In terms of wall shear stress and mass flow rate slight increase have been observed about 1.46% and

Thus, it is clear that MHD has significant effect in blood flow. On the basis of the findings reported here, it may be inferred that the application of an external magnetic field may control blood flow and pressure by increasing or decreasing the magnetic field strength.

6.2 Recommendations for Future Work

Some aspects of this research, I believe, require further investigation in order to provide a thorough picture of the flow conditions within arteries, as well as amelioration to the current approaches. It is recommended that:

The whole design domain is considered a rigid body. The elastic properties of blood vessels can be applied to the wall to get more accurate results. FSI (Fluid solid interface) system can be considered and vessels thickness can be designed to predict how the wall shear stress is changing as well as the wall deformation.

The actual shape of the RBC is oval. It can collide with others and have some shape deformation. This deformation can be investigated in the future.

Refined mesh is necessary to get more accurate outcomes. The entry section of BT, LS and LC arteries sections is not smooth. Improved meshing can be done using meshing software in geometry.

As MHD has effect on blood velocity, pressure and mass flow rate, long term effect on human health in exposur of MHD field can be survey in term of medical science.

REFERENCES

- J. S. Lee and Y. F. Fung. (1970). Flow in locally constricted tubes at low Reynolds numbers, *ASME J. Appl. Mech.* 37,9-16.
- W. L. Oberkampf and S. C. Goh. (1974). Numerical solution of incompressible viscous flow in irregular tubes, *Proc. Int. Conf. on Computer Methods in Non-linear Mechanics*, University of Texas, Austin, pp. 569-579.
- J. M. Terbell. (2003). Mass transport in arteries and the localization of atherosclerosis, *Annual Review of Biomedical Engineering*, vol. 5, pp. 79-118.
- F. Gao, Z. Guo, M. Sakamoto, and T. Matsuzawa. (2006). Fluid-structure interaction within a layered aortic arch model, *Journal of Biological Physics*, vol. 32, no. 5, pp. 435-454.
- D. Mori, T. Hayasaka, and T. Yamaguchi. (2002). Modeling of the human aortic arch with its major branches for computational fluid dynamics simulation of the blood flow, *JSME International Journal, Series C*, vol. 45, no. 4, pp. 997-1002.
- T. Kim, A. Y. Cheer, and H. A. Dwyer. (2004). A simulated dye method for flow visualization with a computational model for blood flow, *Journal of Biomechanics*, vol. 37, no. 8, pp. 1125-1136.
- L. Morris, P. Delassus, A. Callanan et al., Mori, T. Hayasaka, and T. Yamaguchi. (2005). 3-D numerical simulation of blood flow through models of human, *Journal of Biomedical Engineering*, vol. 127, no. 5, pp. 767-775.
- M. Nakamura, S. Wada, and T. Yamaguchi. (2006). Computational analysis of blood flow in an integrated model of the left ventricle and the aorta, *Journal of Biomedical Engineering*, vol. 128, no. 6, pp. 837-843.
- J. Y. Park, C. Y. Park, C. M. Hwang, K. Sun and B. Goo Min. (2007). Pseudo-organ boundary conditions applied to a computational fluid dynamics model of the human aorta, *Computers in Biology and Medicine*, vol. 37, no. 8, pp. 1063-1072.
- N. Shahcheranhi, H.A. Dwyer, A. Y. Cheer, A. I. Barakat, and T. Rutaganira. (2002). Unsteady and three-dimensional simulation of blood flow in the human aortic arch, *Journal of Biomedical Engineering*, vol. 124, no. 4, pp. 378-387.
- B. A. Towfiq, J. Weir, and J. M. Rawles. (1986). Effect of age and pressure on aortic size and stroke distance, *British Heart Journal*, vol. 55, no. 6, pp. 560-568.

- M. Dabagh, P. Jalali, Y. T. Konttinen, and P. Sarkomaa. (2008). Distribution of shear stress over smooth muscle cells in deformable arterial wall, *Medical and Biological Engineering and Computing*, vol. 46, no. 7, pp. 649-657.
- C. Hu, M. Q.-H. Meng, and M. Mandal. (2005). Efficient Magnetic Localization and Orientation Technique for Capsule Endoscopy. *International Journal of Information Acquisition*, vol. 02, no. 01, pp. 23–36.
- M. Ikehata, T. Kawasaki, Y. Suzuki, H. Shimizu, and T. Koana. (2006). Effects of Magnetic Field on Biological Systems. *Quarterly Report of RTRI*, vol. 47, no. 1, pp. 6–11.
- M. V. Hemelrijck, M. Taramasso, C. De Carlo, S. Kuwata, E. Regar, F. Nietlispach, A. Ferrero, A. Weber, and F. Maisano. (2018). Recent advances in understanding and managing aortic stenosis. *F1000Research*, vol. 7, p. 58.
- S. Rashidi, J. A. Esfahani, and M. Maskaniyan. (2017). Applications of magnetohydrodynamics in biological systems-a review on the numerical studies. *Journal of Magnetism and Magnetic Materials*, vol. 439, pp. 358–372.
- S. Tabakova, P. Raynov, N. Nikolov, and S. Radev. (2017). Newtonian and Non-Newtonian Pulsatile Blood Flow in Arteries with Model Aneurysms. *Advanced Computing in Industrial Mathematics*, pp. 187– 197.
- A. Hammoud, E. Y. Sharay, and A. N. Tikhomirov. (2019). Newtonian and non-Newtonian pulsatile flows through carotid artery bifurcation based on CT image geometry. *XLIII Academic Space Conference: dedicated to the memory of academician S.P. Korolev and other outstanding Russian scientists – Pioneers of space exploration*.
- K. M. Khanafer, P. Gadhoke, R. Berguer, and J. L. Bull. (2006). Modelling pulsating flow in aortic aneurysms: effect of non-Newtonian properties of blood. *Biorheology*, vol. 43, pp. 661-679.
- Tse, Z., Dumoulin, C., Clifford, G., Jerosch-Herold, M., Kacher, D., Kwong, R., and Schmidt, E. (2010). MRI-compatible 12-lead ECGs with MHD separation: application to cardiac MRI gating, physiological monitoring and noninvasive cardiac-output estimation. In *Proceedings of 18th Annual Meeting ISMRM, Stockholm* pp. 286.
- Das, C., Wang, G., & Payne, F. (2013). Some practical applications of magnetohydrodynamic pumping. *Sensors and Actuators A: Physical*, 201, 43-48.
- Sankar, D. S., & Lee, U. (2011). FDM analysis for MHD flow of a non-Newtonian fluid for blood flow in stenosed arteries. *Journal of mechanical science and technology*, 25(10), 2573-2581.

- Barnothy, M. F., & Sümegi, I. (1969). Effects of the magnetic field on internal organs and the endocrine system of mice. In *Biological effects of magnetic fields*. Springer US, pp. 103-126.
- Mekheimer, K. S. (2004). Peristaltic flow of blood under effect of a magnetic field in a non-uniform channels. *Applied Mathematics and Computation*, 153(3), pp. 763-777.
- Haldar, K., & Ghosh, S. N. (1994). Effect of a magnetic field on blood flow through an indented tube in the presence of erythrocytes. *Indian Journal of Pure and Applied Mathematics*, 25, pp. 345-345.
- H. Hatami, J. Hatami, and D. D. Ganji. (2014). Computer simulation of MHD blood conveying gold nanoparticles as a third grade non-Newtonian nanofluid in a hollow porous vessel. *Computer Methods and Programs in Biomedicine*, vol. 113, no. 2, pp. 632–641.
- H. Amlimohamadi, M. Akram, and K. Sadeghy. (2016). Flow of a Casson fluid through a locally-constricted porous channel: a numerical study. *Korea-Australia Rheology Journal*, vol. 28, no. 2, pp. 129–137.
- H. Alimohamadi and M. Imani. (2014). Finite element simulation of two-dimensional pulsatile blood flow through a stenosed artery in the presence of external magnetic field, *International Journal for Computational Methods in Engineering Science and Mechanics*, vol. 15, no. 4, pp. 390–400.
- E. E. Tzirtzilakis. (2005). A mathematical model for blood flow in magnetic field,” *Physics of Fluids*, vol. 17, no. 7, article 077103.
- K. S. Mekheimer. (2004). Peristaltic flow of blood under effect of a magnetic field in a non-uniform channels. *Applied Mathematics and Computation*, vol. 153, no. 3, pp. 763–777.
- M. Jain, G. C. Sharma, and A. Singh. (2009). Mathematical analysis of MHD flow of blood in very narrow capillaries. *Inter. J. Eng. Transactions B*, vol. 22, pp. 307–315.
- K. G. Varshney, V. Katiyar, and S. Kumar. (2010). Effect of magnetic field on the blood flow in artery having multiple stenosis: a numerical study. *International Journal of Engineering, Science and Technology*, vol. 2, no. 2, pp. 67–82.
- K. S. Mekheimer, T. Elnaqeeb, M. A. El Kot, and F. Alghamdi. (2016). Simultaneous effect of magnetic field and metallic nanoparticles on a micropolar fluid through an overlapping stenotic artery: blood flow model. *Physics Essays*, vol. 29, no. 2, pp. 272–283.

- T. Elnaqeeb, K. S. Mekheimer, and F. Alghamdi. (2016). Cu-blood flow model through a catheterized mild stenotic artery with a thrombosis. *Mathematical Biosciences*, vol. 282, pp. 135–146.
- T. Elnaqeeb, N. A. Shah, and K. S. Mekheimer. (2019). Hemodynamic characteristics of gold nanoparticle blood flow through a tapered stenosed vessel with variable nanofluid viscosity. *BioNanoScience*, vol. 9, no. 2, pp. 245–255.
- T. Elnaqeeb. (2019). Modeling of au (NPs)-blood flow through a catheterized multiple stenosed artery under radial magnetic field. *The European Physical Journal Special Topics*, vol. 228, no. 12, pp. 2695–2712.
- S. Sharma, U. Singh, and V. K. Katiyar. (2015). Magnetic field effect on flow parameters of blood along with magnetic particles in cylindrical tube. *Journal of Magnetism and Magnetic Materials*, vol. 377, pp. 395–401.
- A. A. Zafar, N. A. Shah, and I. Khan. (2019). Two phase flow of blood through a circular tube with magnetic properties. *Journal of Magnetism and Magnetic Materials*, vol. 477, pp. 382–387.
- N. Ali Shah, D. Vieru, and C. Fetecau. (2016). Effects of the fractional order and magnetic field on the blood flow in cylindrical domains. *Journal of Magnetism and Magnetic Materials*, vol. 409, pp. 10–19.
- S. Kumari, R. Rathee and J. Nandal. (2019). Unsteady peristaltic transport of MHD Fluid through an inclined stenosed artery with slip effect, *International Journal of Applied Engineering Research*, 14(8), pp. 1881-1891.
- M. Sharma, R. Gaur and B. Sharma. (2019). Radiation effect on MHD blood flow through a tapered porous stenosed artery with thermal and mass diffusion, *International Journal of Applied Mechanics and Engineering*, 24(2), pp. 411-423.
- Morris, L., et al. (2005). 3-D Numerical Simulation of Blood Flow through Models of the Human Aorta. *Journal of Biomechanical Engineering*, vol. 127, no. 5, pp. 767–775.
- Abidi, Awatef, et al. (2021). A Review of the Methods of Modeling Multi-Phase Flows within Different Microchannels Shapes and Their Applications. MDPI, Multidisciplinary Digital Publishing Institute.
- J. Lyras and K.G Lee. (2022). Haemodynamic Analysis Using Multiphase Flow Dynamics in Tubular Lesions. *Computer Methods and Programs in Biomedicine*, U.S. National Library of Medicine.

- Shahcheraghi, N., Dwyer, H. A., Cheer, A. Y., Barakat, A. I., and Rutaganira, T. (2002). Unsteady and Three-Dimensional Simulation of Blood Flow in the Human Aortic Arch. *J. Biomech. Eng.*, 124, pp. 378–387.
- Weydahl, E. S., and Moore, J. E. (2001). Dynamic Curvature Strongly affects Wall Shear Rates in a Coronary Artery Bifurcation Model. *J. Biomech.*, 34, pp. 1189–1196.
- Papaharilaou, Y., Doorly, D. J., and Sherwin, S. J. (2002). The Influence of Out-of-Plane Geometry on Pulsatile Flow within a Distal End-to-Side Anastomosis. *J. Biomech.*, 35, pp. 1225-1239.
- Myers, J. G., Moore, J. A., Ojha, M., Johnston, K. W., and Ethier, C. R. (2001). Factors Influencing Blood Flow Patterns in the Human Right Coronary Artery. *Ann. Biomed. Eng.*, 99, pp. 109-120.
- Berthier, B., Bouzerar, R., and Legallais, C. (2002). Blood Flow Patterns in an Anatomically Realistic Coronary Vessel: Influence of Three Different Reconstruction Methods. *J. Biomech.*, 35, pp. 1347–1356.
- Fuchs and Alexander. (2020). Diva Portal. Blood Rheology Modeling Effects in Aortic Flow Simulations.
- Krivovichev, G.V. (2021). Comparison of Non-Newtonian Models of One-Dimensional Hemodynamics. *Mathematics* 2021, 9, 2459.
- Florescu, Maria, et al. (2018). Echocardiographic Assessment of the Aorta. *New Approaches to Aortic Diseases from Valve to Abdominal Bifurcation*, pp. 145–157.
- SINN OTT, Matthew. CLEARY, Paul W. and PRAKASH, Mahesh. (2006). An investigation of pulsatile blood flow in a bifurcating artery using a grid-free method. *Fifth International Conference on CFD in the Process Industries CSIRO*, Melbourne, Australia.
- Jonathan R. (1997). Delaunay refinement mesh generation, PhD thesis, Carnegie-Mellon Univ Pittsburgh Pa School of Computer Science.
- Vasava, Paritosh, et al. (2012). Finite Element Modelling of Pulsatile Blood Flow in Idealized Model of Human Aortic Arch: Study of Hypotension and Hypertension. *Computational and Mathematical Methods in Medicine*, vol. 2012, pp. 1–14.
- Shit, G.C., and Sreeparna Majee. (2018). Computational Modeling of MHD Flow of Blood and Heat Transfer Enhancement in a Slowly Varying Arterial Segment. *International Journal of Heat and Fluid Flow*, vol. 70, pp. 237–246.

- Teferi, Binyam. (2021). Research Paper, Effect of MHD blood flow with velocity thermal and concentration slip boundary layer.
- Oertel. (2004). Biofluid Mechanics of Blood Circulation. (eds) Prandtl's Essentials of Fluid Mechanics. Applied Mathematical Sciences, vol 158. Springer, New York, NY.
- Altintas, Atilla, and Ibrahim Ozkol. (2015), Magnetohydrodynamic Flow of Liquid-Metal in Circular Pipes for Externally Heated and Non-Heated Cases. Journal of Applied Fluid Mechanics, vol. 8, no. 3, pp. 507–514.